Scale-out production of extracellular vesicles derived from natural killer cells via mechanical stimulation in a seesaw-motion bioreactor for cancer therapy

Biofabrication

PAPER

Scale-out production of extracellular vesicles derived from natural killer cells via mechanical stimulation in a seesaw-motion bioreactor for cancer therapy

Jianguo Wu[1,2,3,12], Di Wu[3,12], Guohua Wu[4,12], Ho-Pan Bei[5], Zihan Li[3], Han Xu[6], Yimin Wang[3], Dan Wu[3], Hui Liu[3], Shengyu Shi[3], Chao Zhao[7], Yibing Xu[3], Yong He[8], Jun Li[9], Changyong Wang[10], Xin Zhao[5,*] and Shuqi Wang[1,2,3,11,*]

[1] Department of Respiratory and Critical Care Medicine, Provincial Clinical Research Center for Respiratory Diseases, West China Hospital, Sichuan University, Chengdu 610065, People's Republic of China
[2] National Engineering Research Center for Biomaterials, Sichuan University, Chengdu 610065, People's Republic of China
[3] Institute for Translational Medicine, Zhejiang University, Hangzhou, Zhejiang Province 310029, People's Republic of China
[4] Endocrine and Metabolic Disease Center, The First Affiliated Hospital, and College of Clinical Medicine of Henan University of Science and Technology, Medical Key Laboratory of Hereditary Rare Diseases of Henan; Luoyang sub-center of National Clinical Research Center for Metabolic Diseases, Luoyang 471003, People's Republic of China
[5] Department of Biomedical Engineering, The Hong Kong Polytechnic University, Hong Kong Special Administrative Region of China 999077, People's Republic of China
[6] Department of Building Environment and Energy Engineering, Xi'an Jiaotong University, Xian, Shanxi Province 710049, People's Republic of China
[7] Wellcome Trust-Medical Research Council Cambridge Stem Cell Institute and Department of Clinical Neurosciences, University of Cambridge, Cambridge CB2 0AH, United Kingdom
[8] State Key Laboratory of Fluid Power and Mechatronic Systems, Key Laboratory of 3D Printing Process and Equipment of Zhejiang Province College of Mechanical Engineering, Zhejiang University, Hangzhou, Zhejiang Province 310029, People's Republic of China
[9] State Key Laboratory for Diagnosis and Treatment of Infectious Diseases, National Clinical Research Center for Infectious Diseases, Collaborative Innovation Center for Diagnosis and Treatment of Infectious Diseases, The First Affiliated Hospital, College of Medicine, Zhejiang University, Hangzhou, Zhejiang Province 310003, People's Republic of China
[10] Department of Neural Engineering and Biological Interdisciplinary Studies, Institute of Military Cognition and Brain Sciences, Academy of Military Medical Sciences, Beijing 100850, People's Republic of China
[11] Institute for Advanced Study, Chengdu University, Chengdu 610106, People's Republic of China
[12] These authors contributed equally.
[*] Authors to whom any correspondence should be addressed.

E-mail: xin.zhao@polyu.edu.hk **and** shuqi@scu.edu.cn

Keywords: extracellular vesicles (EVs), natural killer cells (NKs), bioreactor, mechanical stimulation, cancer therapy

Supplementary material for this article is available online

OPEN ACCESS

RECEIVED
22 December 2021

REVISED
9 May 2022

ACCEPTED FOR PUBLICATION
6 July 2022

PUBLISHED
5 August 2022

Abstract

Extracellular vesicles (EVs) derived from immune cells have shown great anti-cancer therapeutic potential. However, inefficiency in EV generation has considerably impeded the development of EV-based basic research and clinical translation. Here, we developed a seesaw-motion bioreactor (SMB) system by leveraging mechanical stimuli such as shear stress and turbulence for generating EVs with high quality and quantity from natural killer (NK) cells. Compared to EV production in traditional static culture (229 $\pm$ 74 particles per cell per day), SMB produced NK-92MI-derived EVs at a higher rate of 438 $\pm$ 50 particles per cell per day and yielded a total number of 2×10^{11} EVs over two weeks via continuous dynamic fluidic culture. In addition, the EVs generated from NK-92MI cells in SMB shared a similar morphology, size distribution, and protein profile to EVs generated from traditional static culture. Most importantly, the NK-92MI-derived EVs in SMB were functionally active in killing melanoma and liver cancer cells in both 2D and 3D culture conditions *in vitro*, as well as in suppressing melanoma growth *in vivo*. We believe that SMB is an attractive approach to producing EVs with high quality and quantity; it can additionally enhance EV production from NK92-MI cells and promote both the basic and translational research of EVs.

1. Introduction

Extracellular vesicles (EVs) have been utilized to deliver specific chemical compounds (e.g. proteins, nucleic acids and metabolites) in cancer therapy (e.g. metastatic breast cancer, lymphoma) due to their enhanced penetrative properties arising from their composition and nanoscale size [1, 2]. Recently, EVs derived from immune cells such as natural killer T cells (NK cells) have shown notable anti-cancer therapeutic potential with wide-spectrum efficacy, which brings new treatment options for cancer patients [3–10]. For example, NK cell-derived EVs (NK EVs) have been demonstrated to harbor tumor inhibitory molecules such as CD56, NCRs, NKG2D, perforin, granulysin, and granzyme A-B, and exert cytotoxic effects on cancer cells through Perforin/Granzymes and Fas–Fas Ligand [11]. Unfortunately, inefficiency in generating functional EVs with high quality and quantity from their parental cells has significantly impeded the development of EV-based fundamental research and clinical translation [12, 13].

To circumvent these challenges, a number of strategies involving biological and chemical cues as well as mechanical approaches have been explored. Certain genes such as STEAP3, syndecan-4 (SDC4), and L-aspartate oxidase (NadB) in cells have been targeted to promote EV production [14]. Cytokines (e.g. TNF-α, IL-8, and leukotriene B4) have also been added in cell culture to increase the production of EVs from neutrophils [15]. These strategies, unfortunately, are overcomplicated in design or they need additional steps to remove the stimulators from the product. In addition, chemical reagents (e.g. cytochalasin B and ethanol), serum deprivation, and hypoxia conditions have been used to increase the EV production [16–19], but they are often compromised by certain cytotoxic effects and may reduce cell viability during long-term cell culture. Inspired by naturally occurring EV release by shear stress in blood vessels [20–23], mechanical stimulation demonstrates its capability to enhance EV production without detrimental effects on cells, while maintaining or even increasing the function of EVs [24–27]. Nevertheless, ultrasound [28] or high-frequency acoustic irradiation [29] may fail to address the reduction in cell viability when the exposure time was over 15 min at their optimized power. Mechanical stretching is also used for enhancing EV production [30]. Yet, mechanical stretching of cell-laden scaffolds often suffers from inner insufficient nutrition and oxygen supply, impeding their scale-up ability in EV production.

To increase EV production in a safe, scalable, and continuous way, in this study, we developed a seesaw-motion bioreactor (SMB) system with continuous fluidic flow for scale-out production of EVs derived from NK-92MI cells for cancer therapy (figure 1). Here, we not only developed a perfusion system for long-term cell culture for EV production, but also revealed the mechanism of enhanced EV production from NK92-MI cells via mechanical stimulation (i.e. seesaw motion). The seesaw-motion in SMB induced sufficient mechanical stimulation including turbulence and shear stress to cells with minimal detrimental effects, activated exocytosis and ultimately generated functional NK EVs with high quality and quantity. Moreover, our SMB enabled a relative long-term EV production under continuous mechanical stress for 11 d, which was significantly longer than the current EV production under chemical, biological or mechanical stimulation (table 1), featuring in potential scale-out EV production. We envision that our SMB can be adapted to produce EVs from a variety of functional cells with high quality and quantity, facilitating the exploration of EV-related basic research and clinical translation.

2. Methods

2.1. Design and fabrication of SMB

The SMB system was designed to have a real-time monitoring, environment-controlled platform (RMECP) (figures 2(A(I)) and S1) and four modular bioreactors. The RMECP platform consisted of a CPU control unit, a temperature control unit, a gas flow control unit, a lighting unit, a UV sterilization unit, a real-time environmental monitoring unit, an operation control unit, and a fluidic flow monitoring unit. The system control unit was developed based on ARM Cortex-M0 in C language, communicating with the sensors in each control unit through UART, I2C and SPI interfaces, and relaying signals through an IO interface to control two electromagnetic valves, a UV sterilization lamp, an illumination lamp, a heating device and a cooling fan, as well as achieving parameter monitoring. The operation control unit facilitated human–computer interactions through a touch screen, and the interface was used to set parameters such as sterilization time, culture temperature, alarm threshold, gas concentration, etc. In a word, the RMECP platform not only ensured the optimal culture conditions, but also controlled the seesaw movement of four modular bioreactors simultaneously.

Each modular bioreactor consisted of two peristaltic pumps, a seesaw-motion shaker, an in-house two-chamber culture device, and a pH sensor and a medium reservoir (figures 2(A(II)) and S1). These components were interconnected via silicone tubes to allow for fluidic flow. The in-house two-chamber culture device (figures 2(A(III)) and S1) was designed to have the upper chamber for NK cell culture and the lower chamber for medium circulation. These two chambers were connected through a PET membrane with a pore size of 5 μm for efficient exchange of nutrients and metabolic wastes, as well as for the passage of EVs to the medium circulation. A porous

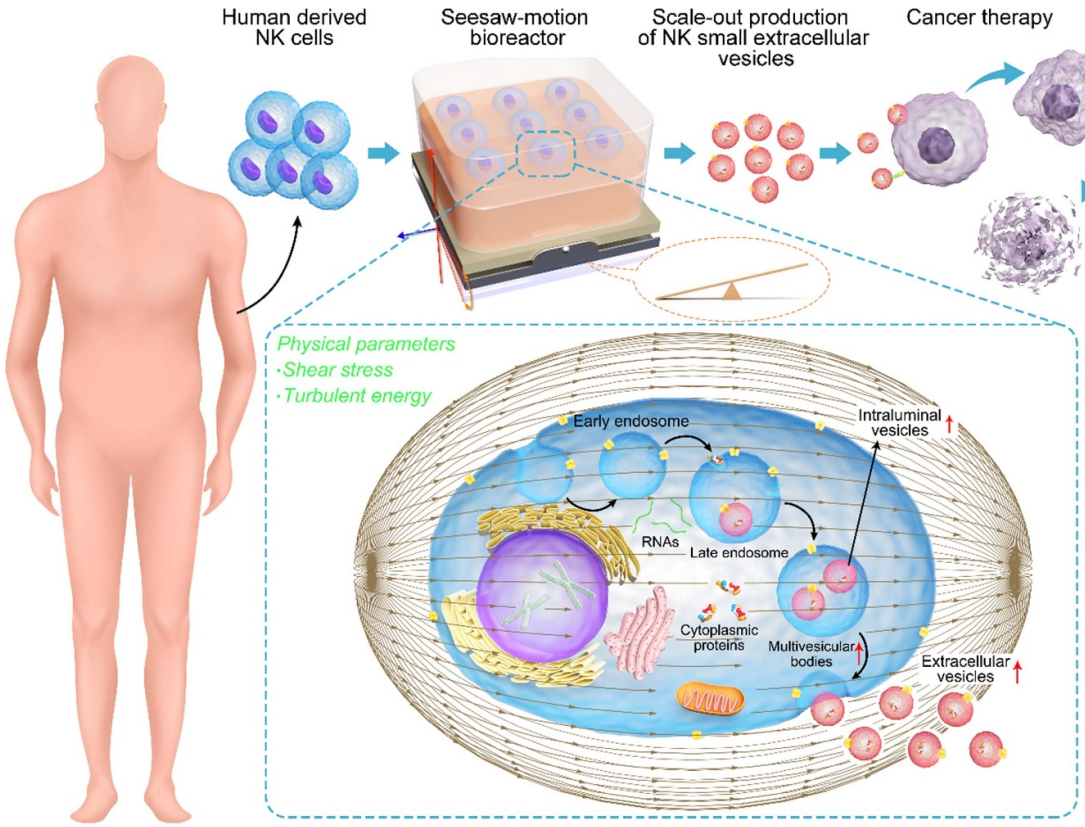

Figure 1. Schematic depicting a seesaw-motion bioreactor (SMB) for scale-out production of NK EVs for cancer therapy. Human derived NK cells are contiguously cultured in SMB for enhanced production of EVs under shaking culture conditions, which confer mechanical stimulations (e.g. shear stress and turbulence) on cells and activate EV biogenesis, resulting in scale-out EV production for cancer treatment.

Table 1. Current EV production under chemical, physical, biological or mechanical stimulations.

Approaches	Cells	Duration	References
TNF-α, IL-8, and Leukotriene B4	Neutrophils	20 min	[15]
Cytochalasin B	HEK293 cells	10–20 min	[16]
Chemical stimulation: Alcohol	Huh7.5 cells	3 d	[17]
Serum deprivation	RPMI 8226 cells; U266 cells, KM3 cells	1 d	[18]
Hypoxia	MDA-MB 231 cells; SKBR3 cells; MCF7 cells	2 d	[19]
Ultrasound	Astrocytes	15 min	[28]
High frequency acoustic wave	U87-MG cells and A549 cells	30 min	[29]
Cyclic stretch	Primary human skeletal muscle cells	2 d	[30]

support structure made of polydimethylsiloxane was placed under the PET membrane to prevent the PET membrane from collapsing. The volume in the upper chamber was 20 ml, the volume in the lower chamber was 250 ml, and the medium reservoir connected to the lower chamber contained 600 ml of RPMI-1640 for continuous medium circulation with the aid of two peristaltic pumps. It should be noted that there was no direct medium infusion to the upper chamber, and mass exchange (e.g. nutrients and metabolites) was only achieved through liquid diffusion cross the PET membrane. A gas exchange port with a 0.22 μm filter was arranged in the upper NK cell culture chamber to ensure efficient gas exchange with the internal environment within SMB. There was no oxygen injection, and 5% CO_2 was maintained with the aid of a CO_2 sensor (MK462, Qin Chuang Sensor Technology Co., Ltd, Shenzhen, China) in the gas flow control unit. In each production batch, four modular bioreactors were used, and a total of 3.48 l (870 ml $\times$ 4) culture medium was obtained to isolate and concentrate EVs. The seesaw movement of the bioreactor is shown in figure 2(B).

2.2. Cell culture

NK-92MI cells from American Type Culture Collection were cultured in RPMI-1640 (Gibco, Melbourne, Australia) supplemented with 1% penicillin-streptomycin (Sangon Biotech, Shanghai, China) and 10% fetal bovine serum (FBS) (Gibco, Melbourne, Australia). It should be noted that FBS was

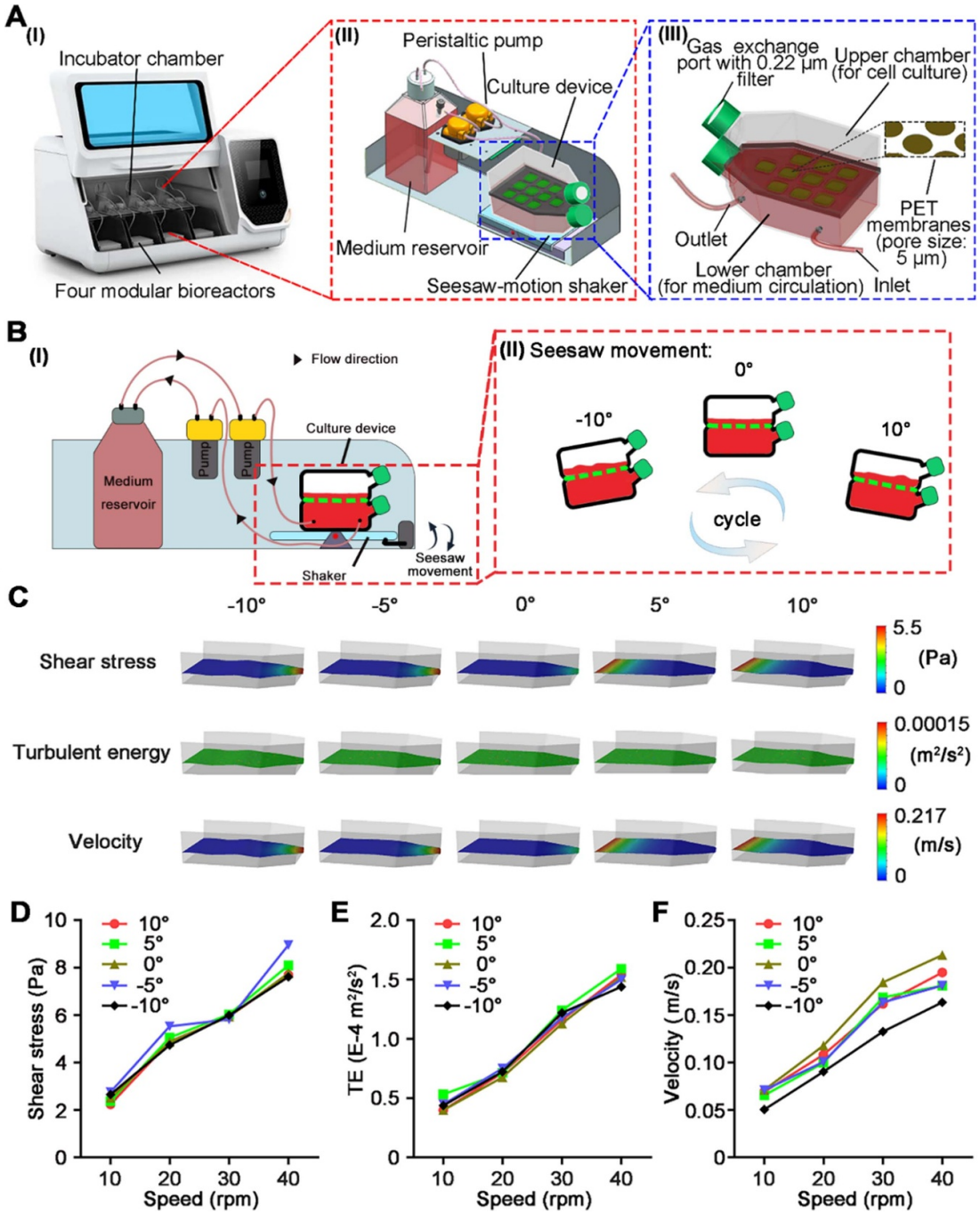

Figure 2. Design of SMB and mathematical modeling of the fluidic dynamics. (A) Design of SMB for continuous production of EVs. (I) Schematic illustration of 4 modular bioreactors with integrated sensors in SMB. (II) Each modular bioreactor consisted of two peristaltic pumps, a seesaw-motion shaker, an in-house two-chamber culture device, a pH sensor and a medium reservoir. (III) Design of the in-house two-chamber culture device for continuous EV production. (B) (I) Illustration the perfusion system in SMB. (II) Illustration of the seesaw motion of the culture chambers. (C) Physical parameters simulated in SMB: shear stress (Pa), turbulent energy ($m^2\ s^{-2}$) and velocity ($m\ s^{-1}$). The color bars show a maximum value of 5.5 Pa, 0.00015 $m^2\ s^{-2}$ and 0.217 $m\ s^{-1}$ for shear stress, turbulent energy and velocity to improve visibility. Shear stress (D), Turbulent energy (E), and Velocity (F) at different angles ($-10°$, $-5°$, $0°$, $5°$, and $10°$) simulated at different shaking speed within SMB.

centrifuged at 110 000 × g for 48 h to remove foreign EVs from FBS. B16F10, A375 and HepG2 cells were obtained from China Center for Type Culture Collection (CCTCC) and were cultured in Dulbecco's modified Eagle's medium (Gibco, Melbourne, Australia) containing penicillin-streptomycin (1%) and FBS (10%). The culturing condition for all cells was 37 °C and 5% CO_2.

2.3. Modeling of mechanical stimulation in bioreactors

To analyze the mechanical stimulation acting on NK cells in quantitative terms, the fluidic flow in SMB was modeled using a computational fluid dynamics package (Fluent, ANSYS Inc., PA, USA). In this model, the governing equations of the mass and momentum conservation were solved to obtain the

detailed distribution of flow velocity, shear strain rate, vorticity, shear stress, energy dissipation, and turbulent energy. The volume-of-fluid method was used to track the deformation and motion of gas-medium free surface to reproduce the physical flow in SMB. To this end, the governing equations were summarized as follow:

$$\frac{1}{\rho_q}\frac{\partial}{\partial t}\left(\alpha_q\rho_q\right)+\frac{1}{\rho_q}\left[\nabla\cdot\left(\alpha_q\rho_q\boldsymbol{u}_q\right)\right]=0$$

$$\frac{\partial}{\partial t}(\rho u)+\nabla\cdot(\rho uu)=-\nabla p+\nabla\cdot\left[\mu\left(\nabla u+\nabla u^T\right)\right]+\rho g+F.$$

Here, ρ is the fluid density; $\boldsymbol{u}$ is the velocity vector; $q=0$ and 1 represent the gas and medium phase, respectively; the volume fraction of the qth phase is denoted by α_q; p is the pressure; $\boldsymbol{g}$ is the gravitational acceleration; and $\boldsymbol{F}$ is the gas-medium surface tension. The SST $k-\omega$ model is used to model the turbulence in SMB, in which the transport equations are given as follow:

$$\frac{\partial(\rho k)}{\partial t}+\frac{\partial(\rho k u_i)}{\partial x_i}=\frac{\partial}{\partial x_j}\left[\left(\mu+\frac{\mu_t}{\sigma_k}\right)\frac{\partial k}{\partial x_j}\right]+X_k-Y_k$$

$$\frac{\partial(\rho\omega)}{\partial t}+\frac{\partial(\rho\omega u_j)}{\partial x_j}=\frac{\partial}{\partial x_j}\left[\left(\mu+\frac{\mu_t}{\sigma_\omega}\right)\frac{\partial\omega}{\partial x_j}\right]+X_\omega-Y_\omega+Z_\omega$$

$$X_k=-\rho\overline{u_i'u_j'}\frac{\partial u_j}{\partial x_i},\ X_\omega=\frac{\alpha}{\nu_t}G_k,\ Y_k=\rho\beta^*k\omega,$$

$$Y_\omega=\rho\beta\omega^2,\ Z_\omega=2(1-R)\frac{\rho}{1.168\omega}\frac{\partial k}{\partial x_j}\frac{\partial\omega}{\partial x_j}.$$

Here, σ_k and σ_ω are the turbulent Prandtl number for the turbulence kinetic energy k and the specific dissipation rate ω. Additional details with regards to these governing equations can be referred to the tutorials of Fluent software. To maintain the second order accuracy for the solution of governing equations for the velocity and pressure, the standard central difference scheme was used for the discretization of all spatial derivatives and the second order upwind scheme was employed for the convective term. In the mathematical model, cell motion is not tracked specifically, since cells flow almost freely with local fluid motion [31]. In our device, the range of Stokes number St in the device at a shaking speed of 20 rpm was between 3.51×10^{-5} and 4.58×10^{-5}, which was smaller than 1, and cell motion was thus neglected. Here, the Stokes number is defined as $\mathrm{St}=(\rho_p{d_p}^2/18\mu)/(L/u)$, where ρ_p is particle mass density, d_p is particle diameter, μ is liquid viscosity, L is the characteristic length of the chamber, and u is the local fluid velocity.

2.4. Characterization of cells cultured in SMB

To apply mechanical stimulations, the cell culture chambers were placed in a built-in shaker with a speed varying from 0 to 40 rpm. For cell culture, 1.0×10^7 NK-92MI cells were inoculated in the upper chamber of the bioreactor containing 20 ml of RPMI-1640 medium. The speed was set from 10 to 40 rpm and cells were cultured for 3 d without medium circulation. After 3 d, 1 ml of culture medium was collected from the upper chamber and imaged under a Zeiss inverted fluorescence microscope (ZEISS, Germany). Image J (National Health Institute, USA) software was then used to measure the size of cell clusters. The culture medium was centrifuged at 1000 g, and the supernatant was harvested for EV isolation through differential centrifugation. The viability of NK-92MI cells at the upper chamber was measured using a Live/Dead assay (Dojindo, Kumamoto, Japan). First, calcein acetoxymethyl ester (Calcein AM) (3 μl) and propidium iodide (PI) (3 μl) solutions were pipetted to 1 ml of PBS for Live/Dead staining. Then, the cells isolated from the upper chamber were incubated with the prepared dye solution in darkness at 37 °C for 15 min. Afterwards, the cells were imaged using a fluorescence microscope, and ImageJ software was used to quantify the number of live/dead cells. The percentage of live cells in the total cells was determined as cell viability. In addition, cell counting was used to measure the proliferation rate of NK-92MI cells cultured in SMB for 11 d. The clusters were dispersed into single cells via pipetting before counting. The proliferation rate was calculated by comparing the number of cells before and after cell culture.

2.5. Real-time PCR (RT-PCR)

For RT-PCR, total RNA was extracted from NK92-MI cells using a MiniBEST Universal RNA Extraction Kit (Takara, Shanghai, China) following the manufacturer's instructions. Then, a PrimeScript™ RT reagent Kit with gDNA Eraser (Takara, Shanghai, China) was used to reversely transcribe the total RNA to cDNA. An amount of cDNA equivalent to 50 ng of total RNA (2 μl) was mixed with 1 μl 10 mM forward primer, 1 μl 10 mM reverse primer, 6 μl nuclease-free water and 10 μl iQ™ SYBR Green Supermix (2 × concentration, Bio-Rad) for RT-PCR set up. The primers of Caspase 3 (ZN-XYW032), Caspase 8 (ZN-XYW035) and Caspase 9 (ZN-XYW036) were purchased from Zhien Biotechnology Co., Ltd (Hefei, China). A CFX Connect™ Real-Time System (Bio-Rad) was used for running RT-PCR and the data were processed by a $2^{-\Delta\Delta Ct}$ method according to a previous work [32].

2.6. Optimization of flow rate for medium circulation

To optimize the flow rate of the medium circulated between the lower chamber and the medium reservoir for long term cell culture, 1.0×10^7 NK-92MI cells were cultured in each modular bioreactor under

medium flow rate of 0.2, 3 or 30 ml min^{-1} at the optimized shaking speed of 20 rpm for 11 d. A volume of 25 ml culture medium from the medium reservoir was harvested at day 3 and day 11. Then, EVs in the culture medium were isolated through differential centrifugation and quantified using a bicinchoninic acid (BCA) kit (Sangon Biotech, Shanghai, China). In addition, the lactate concentration in culture medium, the glucose concentration within NK-92MI cells, and the death percentage were continuously measured every day for 11 d. To this end, 1 ml of cell suspension was sampled from the upper chamber every day and replaced with 1 ml of fresh medium. The cell suspension was centrifuged at 1000 g to pellet the cells. The supernatant was used to measure the lactate concentration using an LA Assay Kit (Solarbio, Beijing, China). The cell pellet was used to measure death percentage and the cellular glucose concentration within NK-92MI cells. Trypan blue (0.4%, Invitrogen, Carlsbad, CA, USA) staining was used to determine the death percentage. Before the staining, the cell clusters were dispersed into single cells via pipetting. The number of unstained (living) cells was divided by the total number of cells to get cell viability. For measurement of cellular glucose concentration, the cell pellet was washed three times using 1 × PBS and resuspended in 1 ml of 1 × PBS. The cells were then lysed via ultrasonication (200 W) for 3 s with an interval of 10 s on ice for 30 times. After water bathing at 95 °C for 10 min, the lysed cells were centrifuged at a speed of 8000 g at 25 °C for 10 min. The glucose concentration within the supernatant was measured using a Glucose Content Test Kit (Solarbio, Beijing, China).

2.7. EV production, isolation and quantification

For EV production in SMB, 1.0×10^7 NK-92MI cells were inoculated in the upper chamber of each modular bioreactor containing 20 ml RPMI-1640 medium, and the shaking speed was set to 20 rpm. During cell culture, the culture medium was flowed at a speed of 30 ml min^{-1}. To present a dynamic course of EV production, 25 ml culture medium from the medium reservoir was harvested every day for 11 d, and subsequently processed through differential centrifugation. In comparison, traditional EV production was performed in flasks, in which 1.0×10^7 NK-92MI cells were inoculated in 20 ml of RPMI-1640 medium and cultured for 3 d.

EVs were isolated using differential centrifugation. After centrifugation for 20 min at a speed of 2000 g at 4 °C to remove big cell debris, the resultant supernatant was transferred into polycarbonate tubes and centrifuged for 30 min at 4 °C at a speed of 10 000 g to remove small cell debris. Finally, the supernatant was centrifuged for 70 min at 4 °C at the speed of 100 000 g. The resultant pellet was washed with 25 ml of PBS and then centrifuged at 4 °C at the speed of 100 000 g for 70 min. After removing the supernatant, 100 μl of PBS was pipetted to resuspend the EVs, and the resultant EVs was stored at −80 °C.

The resultant EVs was quantified using a BCA kit according to the total protein associated with EVs. In brief, 5 μl of EVs isolated from the culture media was tested in parallel with bovine serum albumin (BSA) standard solution. A multifunctional microplate reader (SpectraMax M5, Molecular Devices, San Francesco, CA, USA) was used to measure the absorbance at the wavelength of 562 nm. For BCA measurement, three replicates were collected from four modular bioreactors for each experimental condition. The yield of EVs per cell was calculated by dividing the amount of EV-associated protein against the total cell number.

Nanoparticle Tracking Analysis (NTA) was also used to quantify the amount of EVs. The collected EV solution was first diluted in PBS at a ratio of 1:100, and then the size and number of EVs were measured using Nanosight NS300 (Malvern Instruments Ltd, Malvern, UK). The capture settings for NTA were used as follow: number of captures (5), capture duration (30 s), screen gain (1.0), camera level (15), detection threshold (5), laser type (Blue 488), camera type (sCMOS), and temperature (26.6 °C). For NTA measurement, five videos were captured for each modular bioreactor and four modular bioreactors were used for each experimental condition.

2.8. EV characterization

The purified EVs and NK cells were imaged via transmission electron microscopy (TEM). For imaging EVs, 20 μL EV solution was placed onto a formvar-carbon coated copper electron microscopy grid for 5 min, and filter paper was then used to absorb the extra solution. Next, uranyl acetate (20 μl) was pipetted to conduct negative staining for 1 min. Filter paper was used to dry the liquid, and the grids were examined by operating a JEM-1010 transmission electron microscope (JEOL, Ltd, Tokyo, Japan) at 80 kV. For NK cells, 5×10^6 cells were rinsed in PBS (1 mol l^{-1}) and immersed with glutaraldehyde (2.5%) overnight at 4 °C for TEM imaging. Then, the cell specimens were subsequently fixed using osmium tetroxide (1%) in PBS for 1.5 h and embedded in epoxy resin after dehydration through a graded ethanol series. Staining was performed on ultrathin sections (70 nm) using uranyl acetate and lead citrate. For EV biogenesis analysis, 20 cells from five replicates for each condition were examined under TEM, and multivesicular bodies (MVBs) only containing typical intraluminal vesicles (ILVs) with a characteristic size of 50–150 nm and morphology were taken into account.

2.9. Pharmacological inhibition of exosome biogenesis

Exosome biogenesis was pharmacologically inhibited by culturing NK cells with sulfisoxazole (SFX), which

has been reported effective on inhibiting EV secretion by triggering colocalization of MVBs with lysosomes for degradation [33]. A total number of 1×10^7 cells were cultured in the medium containing 100 μM SFX in SMB, and the shaking speed was set to 0 or 20 rpm. The cells exposed to the medium without SFX in SMB at 0 or 20 rpm was used as control. Following the coculture for 48 h, EVs in the medium were harvested via differential centrifugation and analyzed using NTA.

2.10. Western blot (WB)

NK cells cultured under static condition or in SMB at 20 rpm as well as EVs obtained from these two conditions were lysed using RIPA Lysis Buffer containing 1 mM PMSF protease inhibitor (Solarbio Science & Technology Co., Ltd, Beijing, China) and then centrifuged at 12 000 rpm for 2 min to remove the insoluble materials. Next, the resultant lysate containing 30 μg lysed protein was mixed with 5 $\times$ protein loading buffer (Sangon Biotech, Shanghai, China) and boiled for 5 min. After cooling down on ice, the denatured proteins were then loaded onto SDS-PAGE gel (10%) and processed at 120 V for 100 min. After the separated proteins were transferred to a PVDF membrane (Millipore, Billerica, Ma, USA), and the membrane was blocked with skimmed milk (5% w/v) at room temperature for 2 h, antibodies against CD63, Tsg101, HSC70 or Calnexin (all primary antibodies used were from Abcam, Shanghai, China and diluted at a ratio of 1: 1000) were incubated with the membrane for 12 h at 4 °C. The membrane was then washed five times in TBST buffer and incubated with a horseradish peroxidase (HRP)-coupled secondary antibody (Goat anti-Rabbit, Abcam, Shanghai, China) at room temperature at a dilution ratio of 1:2000 for 1 h. The membrane was washed again five times in TBST buffer, and an ECL exposure solution (Abcam, Shanghai, China) was added for signal development. Bio-Rad chemiluminescence imaging system (Hercules, California, USA) was used to visualize the target proteins.

2.11. Enzyme-linked immunosorbent assay (ELISA)

The concentration of CD63 and SDC4 within NK cells cultured in SMB at 0 or 20 rpm was quantified using ELISA. Following cell culture for 48 h, 3×10^6 cells were harvested and washed three times with 1 $\times$ PBS. The cells were treated by freezing and thawing for five times, and centrifuged at 1500 g for 10 min. The resultant supernatant was analyzed using a human CD63 kit (Elabscience, Wuhan, China) and a human SDC4 kit (Jianglai Biotechnology Co., Ltd, Shanghai, China) following the manufacturers' instructions. The concentration of perforin-1, granzyme A and granzyme B from 100 μg ml^{-1} EVs derived from NK-92MI cells under static culture (EVs-S) and EVs derived from NK-92MI cells in SMB at 20 rpm (EVs-B) were measured using Human perforin 1, Human Granzyme A and Human Granzyme B ELISA kits (Jiyinmei Biotechnology Co., Ltd, Wuhan, China).

2.12. Protein analysis by mass spectroscopy (MS)

After reduction with 50 mM dithiothreitol for 10 min at 95 °C, EVs and cell lysates were alkylated with iodoacetamide at 25 °C for 30 min and covered in foil. Next, trypsin (Promega, Madison, Wisconsin, USA) was used to digest the samples at a ratio of 1:50 (enzyme-to-sample weight) at 37 °C. After 12 h digestion, 10% formic acid (FA) was used to terminate the reaction. Subsequently, the digested peptides were desalted in a ZipTip C18 (P10, Millipore Corporation, Billerica, MA, USA). A SpeedVac (Thermo Fisher, Waltham, MA, USA) was then used to dry the resultant eluent, and the dried samples were reconstituted in 2% acetonitrile (ACN) containing 0.1% FA. The resuspended peptides were loaded into a BEH C18 nanoACQUITY Column (130 Å, 1.7 μm, 75 μm $\times$ 250 mm) and extracted using an elution method at 200 nl min^{-1} for 120 min in 0.1% FA with an escalating gradient of ACN. The resultant peptides were then analyzed using an Orbitrap^{TM} mass spectrometer with a full-mass scan of 300–1800 m/z and a resolution of 70 000. The top 20 peaks were used to perform subsequent fragmentation at an HCD (higher-energy collisional dissociation) of 27% collision energy. The proteomic analysis was carried out at 2.0 m/z isolation width and 35 000 resolution, and the acquired raw data were compared with the human UniProt database (www.uniprot.org/) via MaxQuant.

2.13. Cytotoxicity of NK EVs to cancer cells in 2D condition

To measure the tumor killing effect of NK-derived EVs, *in vitro* cytotoxicity test was carried out in a 96-well plate. To this end, 1×10^5 cells were seeded in each well, and the plates were placed into an incubator for 12 h (37 °C, 5% CO_2). A375 cells were exposed to media containing 0.0 or 9.0 μg of EVs-B for 5 h. The cells were then stained using a Live/Dead kit (Dojindo, Kumamoto, Japan) and assessed using an inverted fluorescence microscope (Zeiss, Jena, Germany). The number of live/dead cells was quantified using ImageJ software to analyze the tumor killing effects of NK-derived EVs. In addition, the apoptosis of cells treated with or without NK-derived EVs were assessed using an apoptosis kit (Biyuntian, Shanghai, China) with the aid of a CytoFLEX LX flow cytometer (Beckman, Brea, California, USA).

To investigate whether the killing effects of NK EVs were tumor-specific, non-tumor liver cells (HepLL) were incubated with 9 μg of NK EVs for 1.5, 5 and 12 h. In addition, liver tumor cells (HepG2) were treated with or without 9 μg EVs derived from

fibroblasts (FB EVs) for 1.5, 5, or 12 h to investigate whether the cytotoxic effects were due to the use of a high density of EVs. The cytotoxic effects of EVs to cells were evaluated using the CCK-8 kit as mentioned above.

2.14. Cytotoxicity of NK EVs on cancer cells in 3D condition

For 3D cell culture, 1×10^6 A375, B16F10, or HepG2 cells were mixed with 100 μl culture medium containing 0.05 g ml^{-1} GelMA (GM-60, Yongqinquan Intelligent Equipment Co., Ltd, Suzhou, China) and 0.0025 g ml^{-1} Lithium phenyl-2,4,6-trimethylbenzoyl phosphonate (LAP, Yongqinquan Intelligent Equipment Co., Ltd, Suzhou, China), and the mixture was exposed to UV light for 10 s [34, 35]. Then, the cells were incubated in media containing 0 or 9.0 μg of EVs-B for 5 h. Finally, the cells were stained using a Live/Dead staining kit and visualized under an inverted fluorescence microscope.

2.15. Animal study

A total of 1×10^6 A375 cells in 100 μl PBS was inoculated intradermally into nude mice (Zhejiang Laboratory Animal Center, Hangzhou, China) to create melanoma bearing mice. After 5 d, the mice were injected intratumorally with 20 μg NK EVs in 50 μl of 0.9% NaCl (referred to the NK EV-treated group) or 50 μl of 0.9% NaCl solution (referred to the control group) every two days. The tumor volume and the body weight of the mice were measured three times a week. All animal care and experiments followed the animal experimentation protocols described by the Animal Care Ethics Committee of Zhejiang University, and this animal study was approved by the Animal Ethics Committee of Zhejiang University (ZJU20200078).

2.16. Histological analysis

The mice were sacrificed on day 17, and the tumors were harvested for histological analysis. The tumor tissues were fixed in 4% paraformaldehyde, embedded in paraffin and cut into slices with a thickness of 7 μm. After deparaffinization and rehydration, the slices were hematoxylin and eosin (H&E) stained or analyzed using a TUNEL kit (Ruchuang bio-tech, China) following the manufacturer's instruction. Additional samples were permeabilized and incubated with rabbit polyclonal antibodies against Ki67 (Dilution: 1:10 000, Proteintech, Rosemont, Illinois, USA) or rabbit polyclonal antibodies against PCNA (Dilution: 1:500, Proteintech, Rosemont, Illinois, USA). After washing with PBS, the tumor sections were stained using biotinylated streptavidin-HRP, 3,3′-diaminobenzidine and hematoxylin. Images were captured using a NIKON ECLIPSE C1 microscope and analyzed using Image Pro Plus 6.0 software.

2.17. Data analysis

The results were expressed by mean ± SD. Multiple comparative analysis was completed via ANOVA, and two-tailed Student's t-test was used to determine the statistical difference by analyzing whether a p-value was less than 0.05 or 0.01. The data analysis was performed using the GraphPad Prism 5 (GraphPad Software Inc., San Diego, California, USA).

3. Results

3.1. Fluid simulation model of SMB

To understand the dynamics of physical stress in SMB and the effects of physical stress on EV production, we conducted computational simulation of fluid dynamics in SMB under different shaking speed. To clearly illustrate the spatial distribution of flow field in the bioreactor, the isocontours of shear stress, turbulent energy, and velocity magnitude were plotted in figure 2(C). The simulation results showed that the maximum shear stress, the maximum turbulent energy, and the maximum velocity magnitude in the bioreactor increased with the shaking speed from 10 to 40 rpm at five different inclination angles (i.e. −10°, −5°, 0°, 5°, and 10°) (figures 2(D)–(F)) although the maximum vorticity and the maximum shear strain rate showed no significant changes with varying shaking speeds (figures S1(B) and (C)). The range of mechanical parameters characterizing fluidic dynamics were summarized as below: 0–8.95 Pa for shear stress, 0–42.05 s^{-1} for shear strain rate, 0–0.21 m s^{-1} for velocity, 0–1.59×10^{-4} m^2 s^{-2} for turbulent energy, 0–42.05 s^{-1} for shear strain rate, and 0–23.97 s^{-1} for vorticity. The above results indicated that this SMB system could induce mechanical stimulation on cells cultured in this system in a controlled manner.

3.2. Effect of shaking speed on NK-92MI cells in SMB

To study the effect of physical stress on NK-92MI cells in SMB, we cultured NK-92MI cells under different shaking speed (10, 20, 30, 40 rpm) without medium circulation for 3 d (figure 3). The bright-field images showed that the NK-92MI cells aggregated in clusters with a mean size of 76.60 ± 20.21 and 87.58 ± 27.11 μm under the shaking speed of 0 and 10 rpm, respectively (figures 3(A) and (C)). Meanwhile, NK-92MI cells remained relatively dispersed with a mean size of 19.44 ± 3.19, 17.55 ± 1.96 and 17.31 ± 2.68 μm at a speed of 20, 30 and 40 rpm, respectively (figures 3(A) and (C)). In addition, Live/Dead staining showed that the cell viability was 98.29 ± 0.40%, 98.17 ± 0.49%, 97.18 ± 1.11%, 96.52 ± 0.99%, and 37.19 ± 4.86% at 0, 10, 20, 30, and 40 rpm, respectively (figures 3(B) and (D)). These results showed that the cell viability remained over 95%, and there was no marked difference in

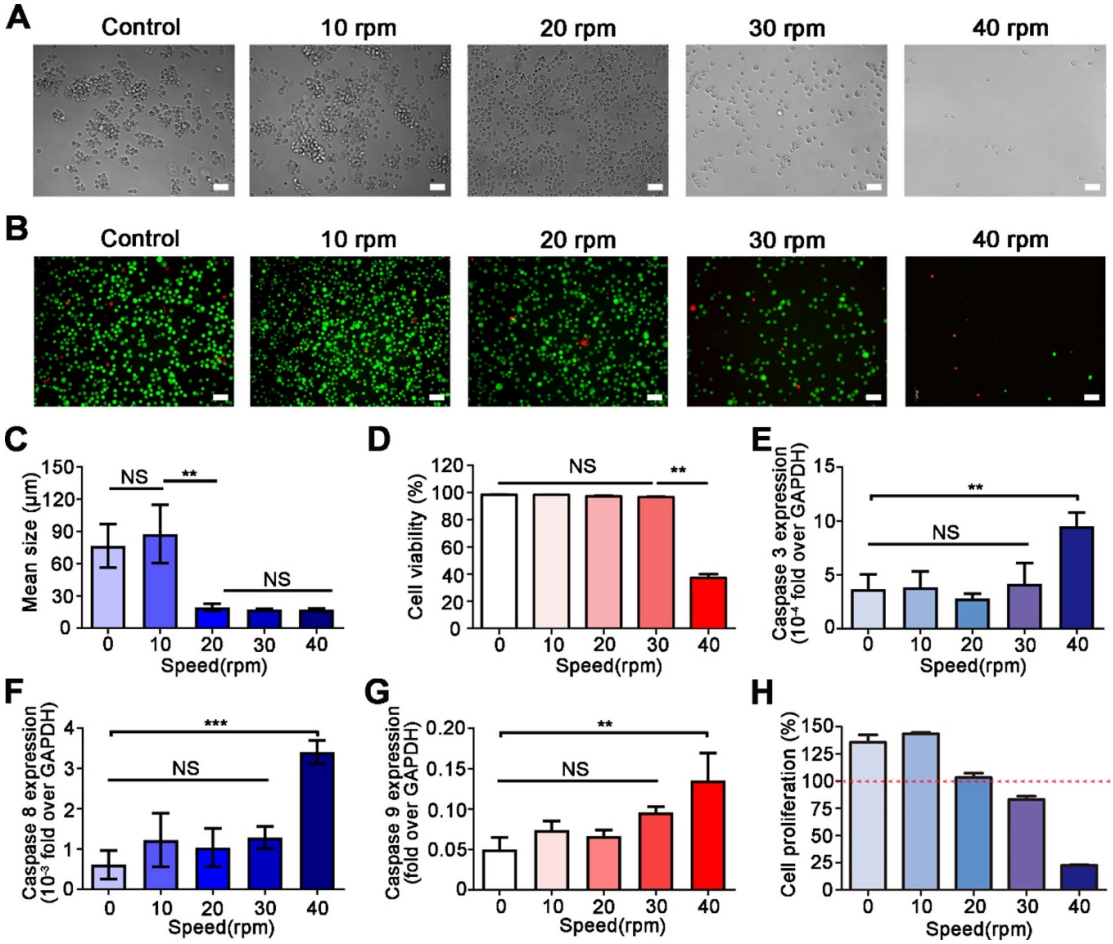

Figure 3. Effect of shaking culture conditions on NK-92MI cells in SMB. (A) Bright-field microscopic images of NK-92MI cell clusters cultured at a shaking speed of 0, 10, 20, 30 and 40 rpm. Scale bar = 50 μm. (B) Live/Dead staining images of NK-92MI cells cultured at a shaking speed of 0, 10, 20, 30 and 40 rpm. Scare bar = 50 μm. (C) Analysis of the mean size of NK-92MI cell clusters cultured at 0, 10, 20, 30 and 40 rpm using ImageJ ($n = 3$). (D) Viability of NK-92MI cells cultured at 0, 10, 20, 30 and 40 rpm ($n = 3$). (E) mRNA expression of Caspase 3 in NK-92MI cells cultured at 0, 10, 20, 30 and 40 rpm ($n = 3$). (F) mRNA expression of Caspase 8 in NK-92MI cells cultured at 0, 10, 20, 30 and 40 rpm ($n = 3$). (G) mRNA expression of Caspase 9 in NK-92MI cells cultured at 0, 10, 20, 30 and 40 rpm ($n = 3$). (H) Daily proliferation percentage of NK-92MI cells cultured under 0, 10, 20, 30 and 40 rpm ($n = 3$). The dotted red line indicates the level of 100% of cell proliferation. Data are presented as mean ± SD. * indicates $p < 0.05$, and ** indicates $p < 0.01$.

the viability of cells cultured at 0, 10, 20 or 30 rpm (figure 3(D)). When the shaking speed increased to 40 rpm, detrimental effects on NK-92MI cells was observed with a significant loss in cell viability (figure 3(D)). RT-PCR results further showed the level of mRNA expression of cell apoptosis related Caspase-3, Caspase-8, and Caspase-9 in NK92-MI cells at the shaking speed of 40 rpm was significantly higher than the static culture, indicative of the activation of cellular apoptosis [36]. There was no significant difference in the level of mRNA expression of these three proteases in the cells cultured at shaking speed lower than 30 rpm, compared to statically cultured NK92-MI cells (figures 3(E)–(G)). Furthermore, cell counting data showed that the cell proliferation rate was 135.7 ± 15.20%, 143.4 ± 2.59%, 103.2 ± 8.93%, 83.00 ± 6.88%, and 22.48 ± 1.40% at the shaking speed of 0, 10, 20, 30, and 40 rpm, respectively (figure 3(H)). There was no detrimental effect found on the aggregation, viability and proliferation of NK-92MI cells at low shaking speed. At a shaking speed of 40 rpm, the viability and proliferation of NK-92MI cells were both less than 50%, and 40 rpm was thus excluded from the following evaluations.

3.3. Effect of shaking speed on NK-92MI derived EVs in SMB

To study the effect of shaking speed on the yield of NK-92MI derived EVs, the amount of EVs was quantified using both NTA and BCA for NK-92MI cells cultured at different shaking speed (0–30 rpm) without medium circulation for 3 d. The NTA results showed that the EV production rose with increasing shaking speed (237 ± 50, 335 ± 24, and 438 ± 50 particles per cell per day at a shaking speed of 0, 10, and 20 rpm, respectively) (figure 4(B)). The rise in the EV production was consistent with the protein measurement data. The BCA quantification results

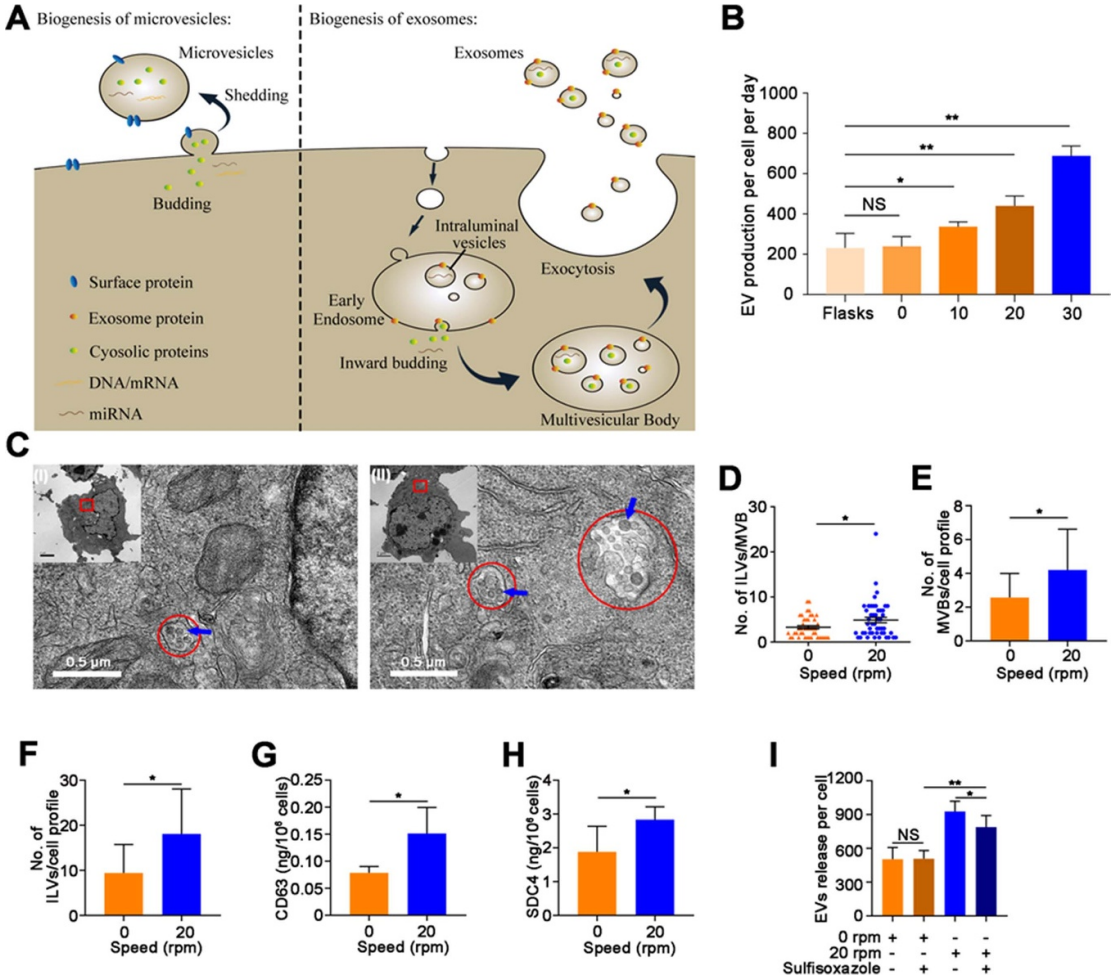

Figure 4. Effect of shaking culture conditions on NK-92MI-derived EVs in SMB. (A) Biogenesis of two kinds of EVs (microvesicles and exosomes). (B) The number of EVs released by NK-92MI cells in flasks or in a modular bioreactor in SMB at a shaking speed of 0, 10, 20 and 30 rpm for 3 d. (C) TEM analysis of typical intraluminal vesicles (ILVs) and multivesicular bodies (MVBs) within NK-92MI cells at 0 (I) and 20 rpm (II). Red boxes are magnified to show MVBs and typical ILVs, which are highlighted in red round circles and blue arrows, respectively. (D) The number of ILVs per MVB within NK-92MI cells at 0 and 20 rpm (mean ± SE, $n = 20$). (E) The number of MVBs per cell profile within NK-92MI cells at 0 and 20 rpm ($n = 20$). (F) The number of ILVs per cell profile within NK-92MI cells at 0 and 20 rpm ($n = 20$). (G) Quantification of CD63 in NK-92MI cells at 0 and 20 rpm ($n = 5$). (H) Quantification of SDC4 in NK-92MI cells at 0 and 20 rpm ($n = 5$). (I) Comparison of EV numbers released from NK-92MI cells treated with or without SFX at 0 or 20 rpm ($n = 5$). Data are presented as mean ± SD. * indicates $p < 0.05$, and ** indicates $p < 0.01$.

Table 2. Protein per particle ratio of EV samples. Note: protein per particle ratio of EVs derived from NK-92MI cells under static culture in flasks or under dynamic culture in SMB at different shaking speed (0, 10, 20 or 30 rpm) based on BCA and NTA measurements. Data are presented as mean ± SD ($n = 3$).

Culture type	Shaking speed (rpm)	Protein per particle ratio (pg per 10^3 particles)
Flask	0	6.89 ± 1.58
SMB	0	8.40 ± 2.43
SMB	10	6.58 ± 0.64
SMB	20	5.68 ± 1.16
SMB	30	4.53 ± 0.59

demonstrated that the amount of NK-92MI derived EVs was 12.69 ± 2.69, 14.28 ± 2.69, 15.96 ± 1.85, and 20.11 ± 1.50 pg per cell under the shaking speed of 0, 10, 20, and 30 rpm, respectively (figure S3(A)). The protein per particle ratio of the EV samples was 8.40 ± 2.43, 6.58 ± 0.64, 5.68 ± 1.16, and 4.53 ± 0.59 pg 10^{-3} particles under the shaking speed of 0, 10, 20, and 30 rpm, respectively (table 2). As the shaking speed of 20 rpm significantly increased EV production per cell with no detrimental effect on cell viability and proliferation, we selected it for the following experiments.

3.4. Characterization of the biogenesis of NK-92MI EVs produced in SMB

To explore the mechanism of how mechanical stimulation affected the EV generation in NK-92MI cells, we assessed the number of EV progenitor subcellular structures including ILVs and MVBs within NK cell aggregates obtained in SMB at 20 rpm using TEM (figures 4(C)–(F) and S4). Under static condition, the number of ILVs per MVBs and the total number of ILVs per cell was found 3.28 ± 0.35 and 9.40 ± 6.33, respectively. Under dynamic culture at 20 rpm, the number of ILVs per MVB increased to 4.90 ± 0.60, and the total number of ILVs per cell rose to 18.08 ± 10.00. These data suggested that there was an upregulation of ILV and MVB formation that led to increased EV biogenesis in mechanically stimulated NK-92MI cells in SMB.

We then performed ELISA quantification of CD63 (a characteristic marker of ILVs) and SDC4 protein (which recruits ALIX and a specialized multiprotein called endosomal-sorting complex to facilitate the formation of MVBs within cells) [33, 37] to characterize the biogenesis of NK-92MI EVs produced in SMB. The results showed that the concentration of CD63 protein in NK-92MI cells at 20 rpm (0.14 ± 0.05 ng per 10^6 cells) was significantly higher than that in cells under static culture (0.07 ± 0.01 ng per 10^6 cells) (figure 4(G)). In addition, the concentration of SDC4 protein in NK-92MI cells at 20 rpm was 2.84 ± 0.38 ng per 10^6 cells, which was remarkably higher than that in cells under static culture (1.88 ± 0.76 per 10^6 cells) (figure 4(H)). The increase in the concentration of both CD63 and SDC4 within NK-92MI cells, together with the TEM analysis, suggested that the mechanical stimulation significantly enhanced the EV biogenesis through the formation of ILVs and MVBs.

As EVs can also be generated through direct outward budding from cell membrane [38], SFX (an inhibitor of exosome secretion [39]) was used to investigate whether the generation of membrane-derived microvesicles was also affected by mechanical stimulation and contributed to the increased EV yield. Our NTA results showed that the number of EVs released from cells with SFX treatment (788 ± 103 particles per cell) was significantly lower than cells without SFX treatment at shaking speed of 20 rpm for 48 h (927 ± 91 particles per cell, mean ± SD, $n = 5$, $p < 0.05$, figure 4(I)). This result indicated that the shedding of exosome was inhibited by SFX. In addition, under SFX treatment for 48 h, the number of EVs released by cells (788 ± 103 particles per cell) at a shaking speed of 20 rpm was significantly higher than that under static culture (507 ± 73 particles per cell, $n = 5$, $p < 0.01$). Considering the shedding of exosomes was significantly inhibited by SFX, the increase of EVs released from NK-92MI cells at shaking speed of 20 rpm was most likely attributed to the enhanced shedding of microvesicles induced by mechanical stimulation (figure 4(H)). In brief, the TEM data and the pharmacological inhibition data suggested that both the biogenesis of exosomes and the shedding of microvesicles are enhanced through continuous mechanical stimulation.

3.5. Production of NK-92MI EVs in SMB

To verify the long-term EV production capability of SMB, NK-92MI cells were placed under dynamic culture at 20 rpm continuously for 11 d using an optimized flow rate to circulate the medium between the lower chamber and the medium reservoir (30 ml min^{-1}, figures 5(A)–(C) and S3). We found that at a low flow rate of 200 μl min^{-1}, the cell viability remained above 90% from day 1 to day 10 but dropped to 79% on day 11 (figure 5(A)), and the cell density dropped from around 0.5 × 10^6 cells per ml to 0.41 × 10^6 cells per ml on day 11 (figure S3(B)). Meanwhile, the cellular glucose concentration decreased from around 0.5 pmol per cell (from day 1 to day 10) to 0.08 pmol per cell on day 11, indicative of an insufficient exchange of nutrient in SMB at a flow rate of 200 μl min^{-1} (figure 5(B)). When the medium flow rate increased to 3 ml min^{-1} or 30 ml min^{-1}, glucose uptake became stable, and cell viability and cell density maintained over a period of 11 d. Moreover, the rate of lactate accumulation in the cell culture chamber decreased at higher flow rate, 30 ml min^{-1} (figure 5(C)). Consequently, 30 ml min^{-1} was selected for long-term cell culture due to its capability to maintain cell viability and cell density, as well as to provide efficient exchange of metabolic waste and nutrient. The BCA protein assay and NTA results demonstrated that EVs were enriched in 4 modular bioreactors gradually over 11 d, and the total production value reached up to 2 × 10^{11} particles per production batch of 3.48 l over 11 d (figures 5(D)–(G)), which was significantly higher than the traditional flask culture (2.74 ± 0.89 × 10^{10} particles in four T75 flasks over 3 d, figure 5(H)). Following ultracentrifugation, NK-92MI EVs harvested from the entire SMB was suspended in 4 ml PBS; the final concentration was 4.93 ± 0.89 × 10^{10} particles ml^{-1}, and the protein content was 279.82 ± 6.7 μg ml^{-1} (figure 5(D)).

3.6. Characterization of NK-92MI EVs produced in SMB

To compare the physical and biological properties of NK-92MI-derived EVs produced by SMB at 20 rpm (EVs-B) and by static culture (EVs-S), TEM, NTA, Western Blot (WB), and mass spectrometry (MS) were performed (figure 6). No significant difference in morphology (figures 6(A(I, II))) or mean size (figure 6(B)) was observed. The distribution of EVs-S and EVs-B measured by NTA were both in the range of 50–350 nm, with peaks around 93.5 nm (figure 6(C(I))) and 119.5 nm (figure 6(C(II))),

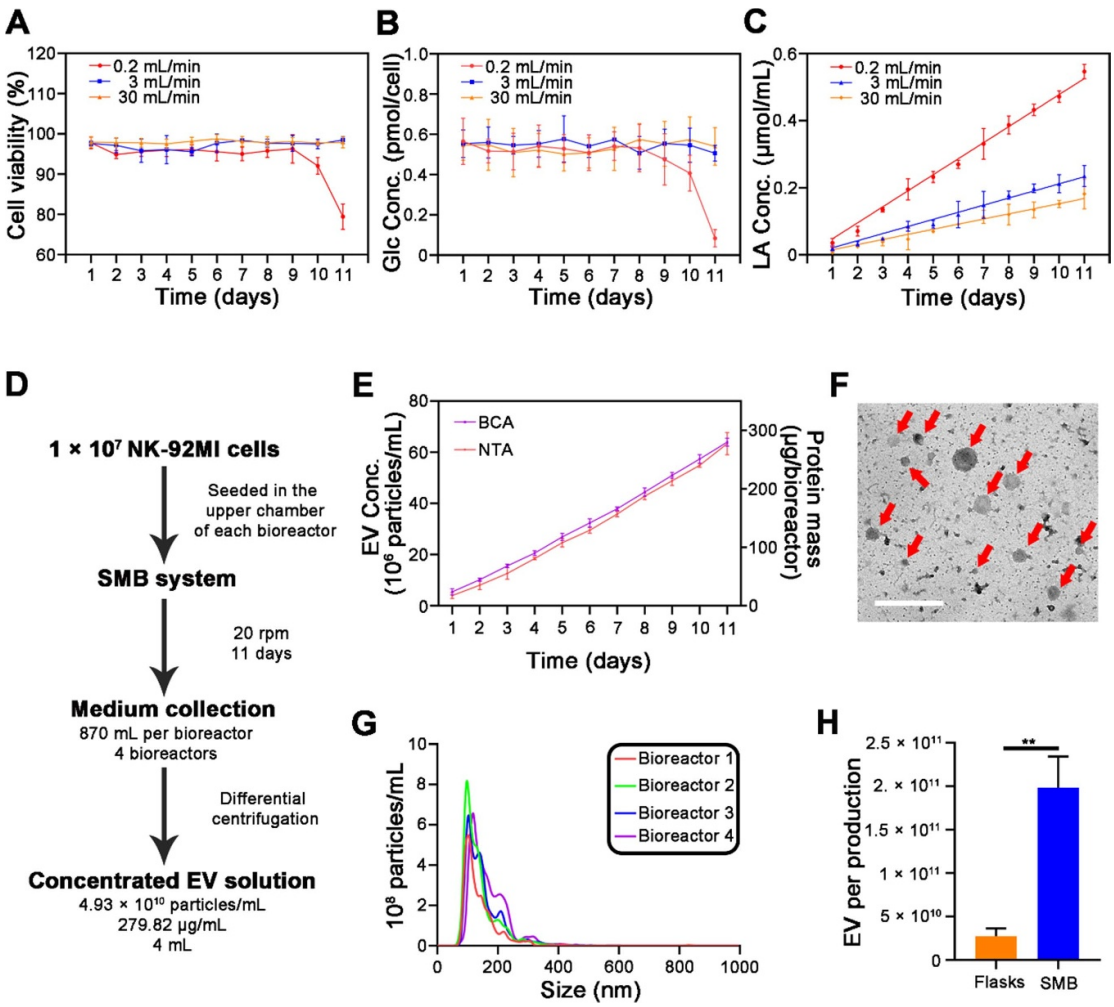

Figure 5. EV production in SMB. (A) Cell viability of NK-92MI cells over a culture period of 11 d at a flow rate of 0.2, 3 and 30 ml min^{-1}. (B) Concentration of glucose (Glc) inside NK-92MI cells over a culture period of 11 d at a flow rate of 0.2, 3 and 30 ml min^{-1}. (C) Concentration of lactic acid (LA) in cell culture chambers within SMB over a culture period of 11 d at a flow rate of 0.2, 3 and 30 ml min^{-1}. (D) Flow chart showing the process of EV production in SMB. (E) Time-response curves presenting the dynamic course of EV production from day 1–11. The yield of EVs was quantified by measuring total protein mass (BCA) and vesicle numbers (NTA). (F) Negative staining of concentrated EVs under TEM (scale bar = 500 nm). (G) NTA analysis of EVs produced by four modular bioreactors in SMB (each curve was obtained by averaging 5 representative videos). (H) The total number of EVs produced in SMB compared to traditional T75 flasks. Data are presented as mean ± SD ($n = 3$). * indicates $p < 0.05$, and ** indicates $p < 0.01$.

respectively. WB revealed that both TSG101 and HSC70 proteins, which are the regulators of vesicular trafficking, were expressed in all cells and EV samples. In addition, both types of EVs exhibited CD63, a benchmark surface protein of EVs. However, calnexin, an endoplasmic reticulum marker naturally in cell lysate, was not found in EV samples (figure 6(D)). This suggested that the collected EV samples from cell culture had negligible cellular debris contamination.

Additionally, MS results showed that the EVs obtained from both SMB and static culture shared 130 different kinds of proteins, and the top 20 enriched proteins were listed in the heatmap (figures 6(E) and (F)). In particular, Perforin is a pore forming cytolytic protein found in the granules of cytotoxic T lymphocytes (CTLs) and NK cells, and the pores formed by it allow for passive diffusion of a family of pro-apoptotic proteases known as granzymes (e.g. granzyme A and B) into target cells to induce cell apoptosis [40]. The concentrations of perforin, granzyme A and granzyme B were thus measured to indicate the potential mechanism of anti-tumor by NK-92MI EVs. In 100 μg ml^{-1} EVs-S, the concentration of perforin, granzyme A and granzyme B was found 1.42 ± 0.05, 1.23 ± 0.07, and 1.53 ± 0.20 ng ml^{-1}, respectively. In comparison, the concentration of perforin, granzyme A and granzyme B in 100 μg ml^{-1} EVs-B was 1.48 ± 0.06, 1.31 ± 0.05, and 1.59 ± 0.13 ng ml^{-1}, respectively. There was no significant difference in the concentration of these three proteins in EVs produced in static culture or SMB (figure 6(G)). These results indicated that the shaking culture conditions maintained the EV morphology, structure and constitution.

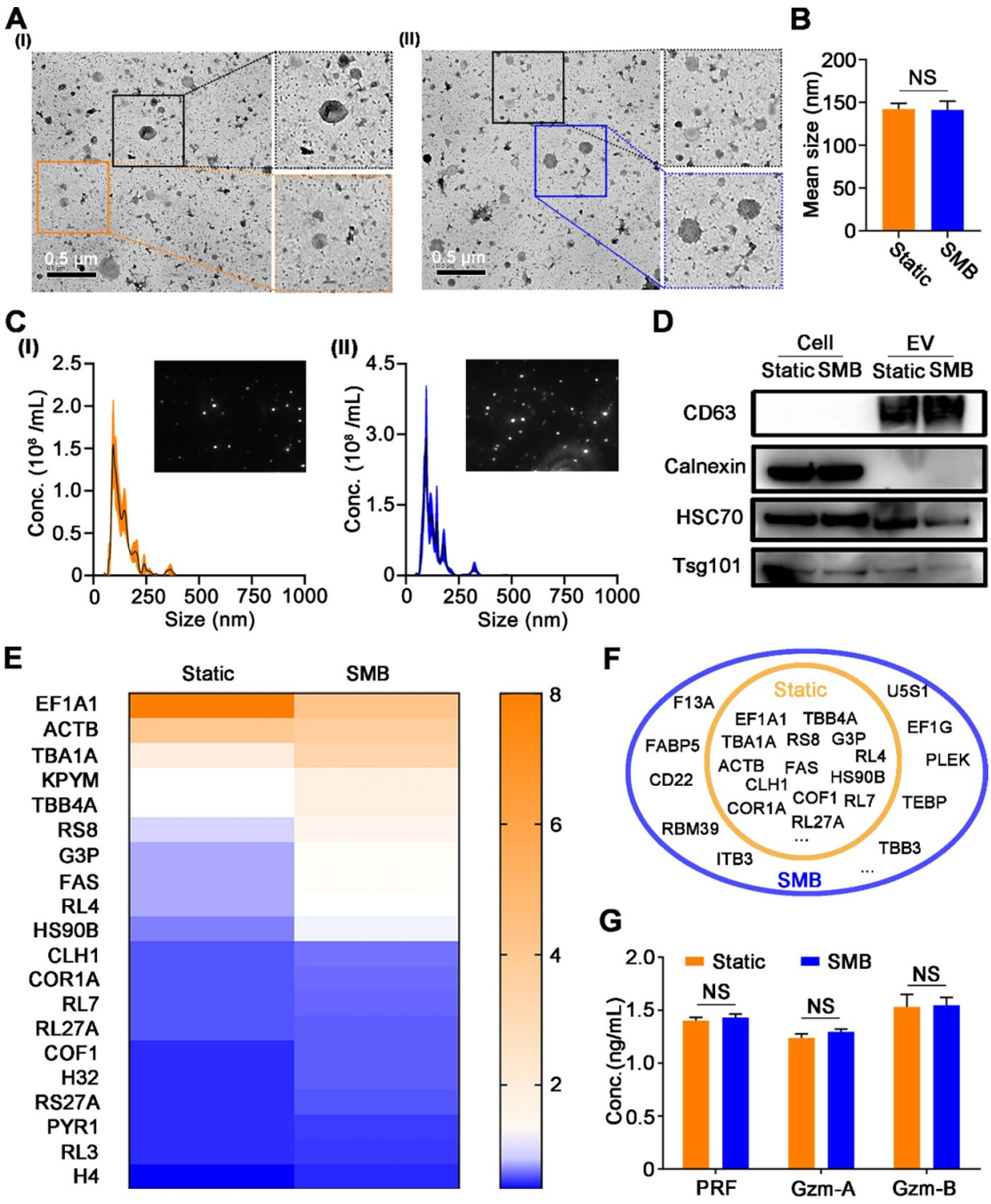

Figure 6. Characterization of NK-92MI derived EVs from static culture or SMB (20 rpm). (A) Representative TEM images of EVs-S (I) or EVs-B (II). The boxes are magnified to show typical EVs. (B) Mean size of EVs-S and EVs-B measured using NTA ($n = 3$). (C) NTA analysis of the size distribution of EVs-S (I) and EVs-B (II) in 200 μl PBS. Five videos were captured from each sample for EV analysis. (D) Western blot analysis of isolated NK-92MI-derived EVs and their parental cells from static culture or SMB, in which 30 μg of protein was loaded in each lane and probed with antibodies against CD63, Calnexin, HSC70 and Tsg101. (E) Top 20 proteins identified by LC–MS/MS of EVs derived from NK-92MI cells generated through static culture or SMB. (F) Venn diagram showing the protein content identified in EVs-S and EVs-B. (G) Concentration of perforin (PRF), granzyme A (Gzm-A) and B (Gzm-B) in EV samples (static culture and SMB) measured using ELISA ($n = 3$). Data are presented as mean $\pm$ SD.

3.7. *In vitro* anti-cancer efficacy of NK-92MI-derived EVs in SMB

NK-92MI EVs are characterized by their wide range of anti-cancer efficacy and high specificity to cancer apoptosis [41]. To investigate the anti-tumor effects of NK-92MI EVs-B compared with their static counterpart, 9 μg EVs-B or EVs-S were cultured with B16F10 cells, and 0 μg treatment served as a negative control (figures 7(A) and (B)). Compared to the negative control, the cell viability of B16F10 cells treated with EVs-S was 71.78 $\pm$ 4.51%, which was comparable to that treated with EVs-B (72.75 $\pm$ 3.50%). These data indicated that both types of EVs exerted comparable anti-tumor efficacy on B16F10 cells.

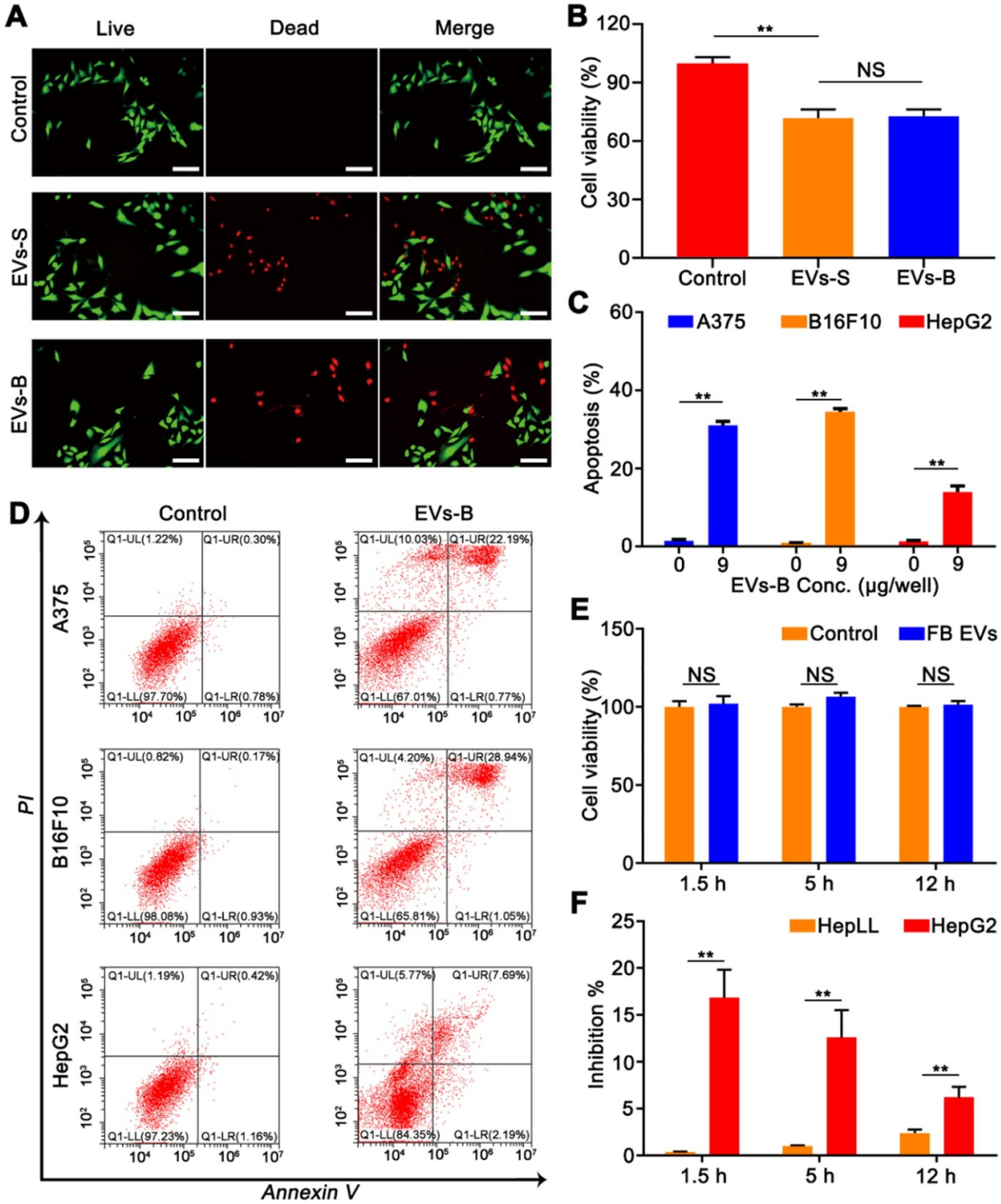

Figure 7. Tumor killing effect of NK-92MI-derived EVs under 2D condition. (A) Live/dead staining images of A375 after incubation for 5 h with 9 μg NK EVs-S or EVs-B ($n = 3$). Live and dead cells are shown in green and red, respectively. Scale bar = 200 μm. (B) Cell viability of A375 analyzed using ImageJ ($n = 5$). (C) Analysis of apoptosis induced by NK-92MI-derived EVs (0 or 9 μg) in A375, B16F10, and HepG2 ($n = 3$). (D) Detection of apoptosis in A375, B16F10 and HepG2 after coculture with or without 9 μg NK-92MI EVs using flow cytometry. (E) Viability of HepG2 cells treated with 9 or 0 (control) μg FB EVs for 1.5, 5 or 12 h ($n = 3$). (F) Inhibition effect of 9 μg NK-92MI EVs on cell viability of non-tumor liver cells (HepLL) and liver cancer cells (HepG2) ($n = 3$). Data are presented as mean ± SD. ** indicates $p < 0.01$.

To further assess the anti-tumor efficacy of EVs-B, three tumor cell lines (A375, B16F10 and HepG2 cells) were incubated with or without EVs for 5 h. Flow cytometry results showed that with EV treatment, the proportion of apoptotic cells among B16F10, A375, or HepG2 cells (31.06 ± 1.75%, 34.40 ± 1.59% and 13.96 ± 2.71%, respectively) was significantly higher than that without EV treatment (1.45 ± 0.60%, 0.93 ± 0.09%, and 1.35 ± 0.37%, respectively) (figures 7(C) and (D)). These results were further supported by Live/Dead staining and CCK-8 assay both under 2D (on 96 well plates) and 3D conditions (in GelMA hydrogels) (figure S5 and S6). Of note, the tumor killing efficacy was not caused by the high density of EVs, since the viability of HepG2 was not affected by the addition of FB-derived EVs (figure 7(E)). To further understand whether the killing efficacy of EVs-B was specific for tumor cells, HepG2 cells (liver cancer cells) and HepLL cells (non-tumor liver cells) were treated with

9 μg EVs-B for 1.5, 5 and 12 h. The cell viability of HepG2 cells was significantly inhibited after EV treatment, and the inhibition percentage was 16.83 $\pm$ 5.19%, 12.58 $\pm$ 5.07%, and 6.16 $\pm$ 2.01%, respectively (figure 7(F)). In comparison, negligible inhibition percentage (0.33 $\pm$ 0.15%, 0.95 $\pm$ 0.21%, and 1.01 $\pm$ 0.82%, respectively, figure 7(F)) was observed on HepLL cells, indicating that the EVs-B have a specific tumor-killing effect. The above results demonstrated that EVs-B have specific tumor-killing effect on multiple tumor cells under both 2D and 3D culture conditions.

3.8. *In vivo* anti-cancer efficacy of NK EVs produced in SMB

The therapeutic effect of EVs produced in SMB was investigated through *in situ* injection of EVs into nude mice grafted with human-derived melanoma (figures 8 and S7). The A375-bearing nude mice were treated with 20 μg EVs at the tumor site every two days or with an equal volume of 0.9% sodium chloride (NaCl) ($n = 6$). A significant difference in the tumor size was observed from day 7 to 17; the tumor volume in the EV-treated group was significantly smaller than that in the control group ($p < 0.05$, figure 8(A)). On day 17, the tumor volume in the EV-treated group was 370.96 $\pm$ 200.27 mm^3, while the tumor volume in the control group was much larger (637.00 $\pm$ 95.64 mm^3) (figure 8(A)). In addition, the tumor weight in the EV-treated group (0.20 $\pm$ 0.10 g) was significantly lower than that in the control group (0.42 $\pm$ 0.07 g) on day 17 (mean $\pm$ SD, $p < 0.01$, figures 8(B(I, II))). Of note, during the entire animal study, the body weight of mice in the EV-treated group showed no significant difference from the control group, indicating that the NK EVs had no detrimental effect on the growth of nude mice. Taken together, the NK EVs produced in SMB were not only safe for administration to mice, but also effective in suppressing human melanoma.

The tumor-suppression effect of NK EVs produced in SMB was further evaluated via analysis of tumor tissues. The hematoxylin and eosin (H&E) staining results showed that the cell density in NK EV-treated tumor was significantly lower than the control tumor (figures 8(C) and (D(I))). In addition, NK EVs significantly downregulated the expression of Ki67 (a proliferation-associated antigen) and a proliferating cell nuclear antigen (PCNA) in tumors (figure 8(C)). The immunohistochemistry (IHC) staining results showed that 55.19% of tumor cells were Ki67 positive and 93.40% were PCNA positive in the control group, whereas only 34.41% of tumor cells were Ki67 positive and 78.50% were PCNA positive in the EV-treated group (figures 8(D(II, III))). Furthermore, based on the terminal deoxynucleotidyl transferase dUTP nick end labeling (TUNEL) results, NK EVs were effective in inducing apoptosis in 29.17% tumor cells, whereas no evident apoptotic cells were observed in the control group (figures 8(C) and (D(IV))). These results indicated that the NK EVs produced in SMB could substantially suppress tumor growth via inhibiting their proliferation and inducing apoptosis in tumor cells *in vivo*. Altogether, the *in vitro* and *in vivo* anti-cancer efficacy results demonstrated that the shaking culture condition did not exert detrimental effect on the biological function of produced EVs.

4. Discussion

EVs have increasingly become an important research avenue in translational medicine, and they have been recently used as a new therapeutic platform for tissue regeneration [42], neurodegenerative diseases [43, 44], and cancer [45, 46]. However, inefficiency of their generation in cells have dampened their development in both basic research and clinical translation. Mechanical forces play a vital role in a wide range of cellular activities including EV biogenesis [21–23, 47–49]. Bearing this in mind, we developed a custom-designed SMB and studied how mechanical stimulation arising from controlled fluid flow affected EV biogenesis in SMB. The mathematical simulation results clearly suggested that this SMB system can be used to induce mechanical stimulations on cells in a controlled manner. Indeed, the mechanical stimulation triggered the enhancement of the cellular biogenesis of NK EVs. This increased cellular biogenesis may be due to the increased tension of the cell membrane induced by mechanical forces. When NK cells were cultured under dynamic flow conditions in SMB, the folds and blebs on the cell membrane may become flattened, leading to the depletion of membrane reservoir and increased membrane tension [50, 51]. As a result, trafficking and exocytosis may be activated in cells to restore the membrane reservoir [52, 53], which may ultimately lead to the increased biogenesis of EVs in SMB. In this study, the velocity, turbulence and shear stress were altered together for increased EV production. However, the individual role of velocity, turbulence and shear stress on cell culture and EV production would be ideally further explored to better understand EV biogenesis under single mechanical stimulations.

The SMB can efficiently enhance the biogenesis of NK EVs. Over a 11 days' production period at the optimized shaking speed and medium flow rate, the total production of NK-92MI EVs in SMB reached up to 2 $\times$ 10^{11} particles which could support a treatment of NK EVs on seven mice for 17 d, and this production was significantly higher than that produced in flasks (2.74 $\pm$ 0.89 $\times$ 10^{10} particles). The production of EVs in SMB could be further scaled out by replacing the culture medium in the medium reservoir with continuous long-term refreshing cell culture medium. Under flow conditions in SMB, metabolic waste generated by cells can be removed from

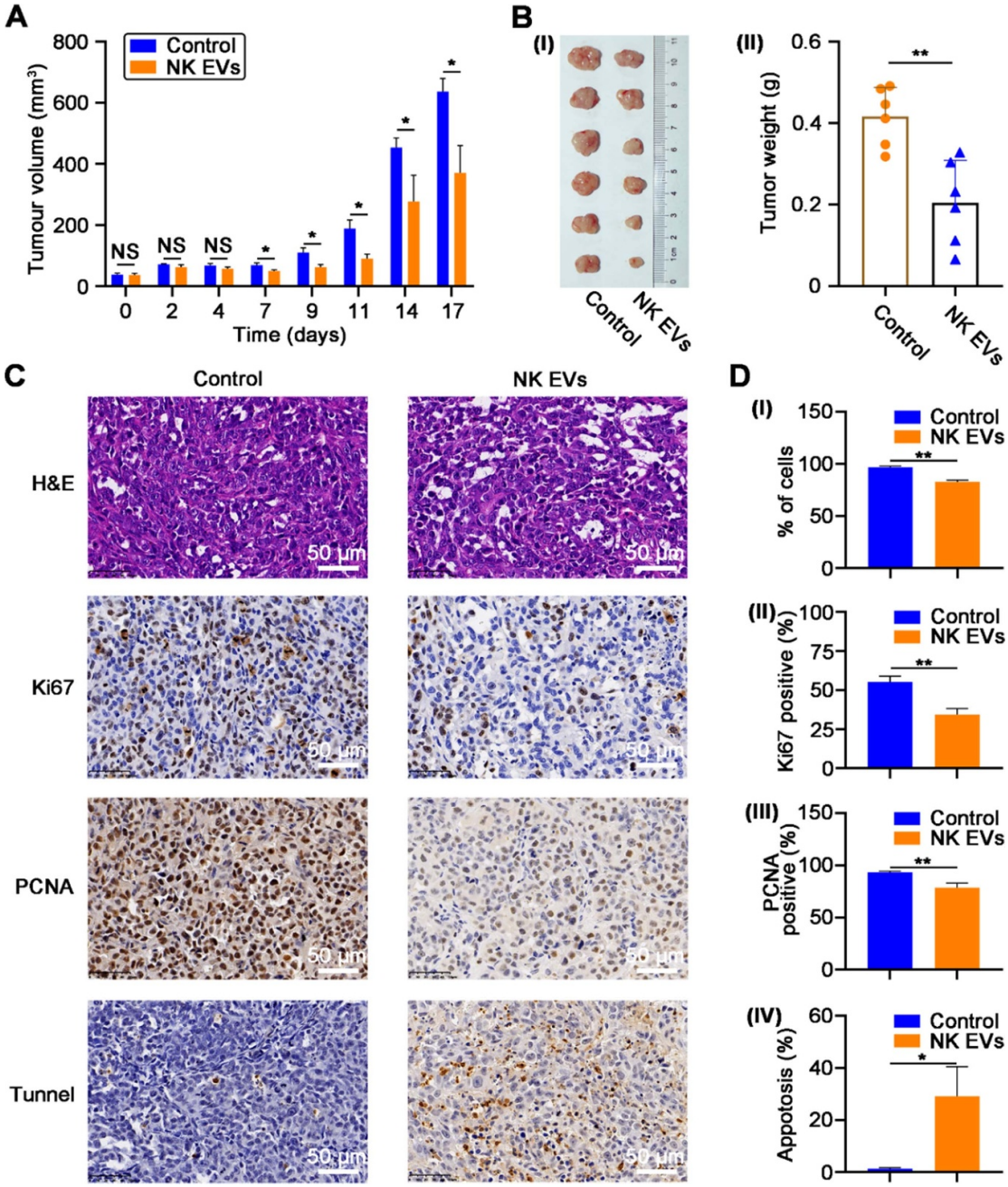

Figure 8. Therapeutic effect of NK-92MI-derived EVs on human-derived melanoma in mice. (A) Comparison of the tumor volume in mice treated with or without EVs. The mice were injected with 20 μg NK-92MI EVs or an equal volume of 0.9% NaCl every two days (starting from day 1) ($n = 6$). (B) Size (I) and weight (II) of melanoma tumors harvested from the EV-treated and control group on day 17. (C) Representative images of H&E, IHC and TUNEL staining of tumor tissues from the two groups. (D) (I) Analysis of the percentage of tumor cells via H&E staining ($n = 6$). (II) Assessment of Ki67 positive cells in tumors ($n = 6$). (III) Assessment of PCNA positive cells in tumors ($n = 6$). (IV) Analysis of the percentage of apoptotic cells in tumor tissue via TUNEL staining ($n = 6$). Data are presented as mean ± SD. * indicates $p < 0.05$, and ** indicates $p < 0.01$.

the upper chamber, and sufficient nutrient can be supplied by circulating medium across the PET membrane in SMB. In addition, most cells were trapped in the upper chamber (figure S8) while EVs could traverse the membrane between the upper and the lower chamber of the culture device and accumulate in the medium reservoir due to the small size of EVs. These factors lay the foundation for long-term EV production in SMB by increasing the working volume. As a result, scalable EV production could be achieved through extended culture period in SMB. Moreover, the cell density can be potentially increased for enhancing EV production in SMB owing to efficient mass exchange via diffusion under flow cell culture condition. As such, this SMB potentially allows for enhanced EV production at higher cell density. Altogether, our SMB is not only able to scale out EV production by increasing the EV production per cell, but also permits scalable EV production by increasing the working volume of cell culture medium and

cell density during the continuous flow-based cell culture.

SMB was found able to increase the EV production per cell and allowed for scalable EV production, while maintaining the structure and function of EVs. NK EVs, produced in either dynamic or static manner, were shown to share similar morphology (figures 6(A)–(C)) and key tumor-killing factor profile (figure 6(G)), as well as to exert similar therapeutic effects on melanoma cells in 2D *in vitro* experiments (figures 7(A) and (B)). Furthermore, we demonstrated the capability of NK EVs produced under mechanical stimulations to kill cancer cells *in vitro* and suppress tumor growth *in vivo*. Nevertheless, it should be borne in mind that mechanical stimulation might alter the expression of some key proteins which regulate signaling pathways and lead to bioactive changes [24, 25].

The ability to produce high quantity and high quality EVs endows SMB with a potential wide usage in EV- based research. In this study, our SMB was applied to produce human derived NK EVs for an allogenic treatment on nude mice. Administration of allogeneic NK EVs is practical for clinical translation, as the NK cell line is easy to obtain. Particularly, the administration of allogeneic NK cells has proven clinically safe in patients for anti-tumor therapy [54–58]. Although administration of autologous NK EVs might not be always available due to the diseased conditions in patients, it is the prime choice for patient treatment. In this case, the number of NK cells extracted from patients is generally limited [59]. With mechanical stimulation under a dynamic culture condition, cells at a relatively low density can maintain their viability and demonstrate enhanced EV production. Thus, our SMB would be valuable for autologous NK EV production. In addition to allogeneic and autologous NK cells, there is a myriad of applications that calls for efficient production of high quality EVs for research or clinical therapy. For example, SMB can be potentially used in producing EVs derived from gene-modified NK cells, where neuron-specific rabies virus glycoprotein (RVG) peptides are expressed, for treatment of glioma [60].

5. Conclusion

In this study, we developed a novel see-saw motion bioreactor based on continuous mechanical stimulation (e.g. shear stress and turbulence) arising from controlled fluidic flow to increase the efficiency of EV generation in cells in a scale-out manner. The SMB significantly enhanced the EV biogenesis in NK-92MI cells, and the efficiency of EV production in NK-92MI cells substantially increased up to 438 ± 50 particles per cell per day, compared to traditional flask culture (229 ± 74 particles per cell per day). In addition, the total production reached up to 2×10^{11} particles over a 11 day culture period. Most importantly, the NK derived EVs in the SMB was found comparable to those generated through static culture in terms of morphology, structure, and function, despite the differences in the protein constitution; they also clearly demonstrated cancer-killing effects both *in vitro* and *in vivo*. To facilitate EV-based research, our system can be adapted and scaled up to several orders of magnitude when considering key parameters such as flow rate, cell type, cell density, mass exchange between culture chambers and medium reservoir, etc. This will facilitate the exploration of EV-related basic research and clinical translation.

Data availability statement

All data that support the findings of this study are included within the article (and any supplementary files).

Acknowledgments

Prof. Shuqi Wang would like to acknowledge the supports from General Program from the National Natural Science Foundation of China (31871016), National Key Research and Development Program (2016YFC1101302), National Key Scientific Instrument and Equipment Development Projects from the National Natural Science Foundation of China (61827806). Prof. Xin Zhao would like to acknowledge the start-up fund (1-ZE7S), central research fund (G-YBWS) and intra-faculty fund (1-ZVPC) from The Hong Kong Polytechnic University. We also acknowledge the technical support from Mr. Wangyao Li, Xiaoxiong Zhao, and Jicheng Wu.

ORCID iDs

Yong He https://orcid.org/0000-0002-9099-0831
Xin Zhao https://orcid.org/0000-0002-9521-7768

References

[1] Cao H, Wang H, He X, Tan T, Hu H, Wang Z, Wang J, Li J, Zhang Z and Li Y 2018 Bioengineered macrophages can responsively transform into nanovesicles to target lung metastasis *Nano Lett.* **18** 4762–70
[2] Ingato D, Edson J A, Zakharian M and Kwon Y J 2018 Cancer cell-derived, drug-loaded nanovesicles induced by sulfhydryl-blocking for effective and safe cancer therapy *ACS Nano* **12** 9568–77
[3] Hoshino A *et al* 2015 Tumour exosome integrins determine organotropic metastasis *Nature* **527** 329–35
[4] Kalluri R 2016 The biology and function of exosomes in cancer *J. Clin. Invest.* **126** 1208–15
[5] Jang S C, Kim O Y, Yoon C M, Choi D S, Roh T Y, Park J, Nilsson J, Lotvall J, Kim Y K and Gho Y S 2013 Bioinspired exosome-mimetic nanovesicles for targeted delivery of chemotherapeutics to malignant tumors *ACS Nano* **7** 7698–710
[6] EL Andaloussi S, Maeger I, Breakefield X O and Wood M J A 2013 Extracellular vesicles: biology and emerging therapeutic opportunities *Nat. Rev. Drug Discov.* **12** 348–58

[7] Ohno S *et al* 2013 Systemically injected exosomes targeted to EGFR deliver antitumor microRNA to breast cancer cells *Mol. Ther.* **21** 185–91

[8] Lener T *et al* 2015 Applying extracellular vesicles based therapeutics in clinical trials—an ISEV position paper *J. Extracell. Vesicles* **4** 30087

[9] Lan J *et al* 2019 M2 Macrophage-derived exosomes promote cell migration and invasion in colon cancer *Cancer Res.* **79** 146–58

[10] Choo Y W *et al* 2018 M1 macrophage-derived nanovesicles potentiate the anticancer efficacy of immune checkpoint inhibitors *ACS Nano* **12** 8977–93

[11] Pace A L D, Tumino N, Besi F, Alicata C, Conti L A, Munari E, Maggi E, Vacca P and Moretta L 2020 Characterization of human NK cell-derived exosomes: role of DNAM1 receptor in exosome-mediated cytotoxicity against tumor *Cancers* **12** 661

[12] Li X, Corbett A L, Taatizadeh E, Tasnim N, Little J P, Garnis C, Daugaard M, Guns E, Hoorfar M and Li I T 2019 Challenges and opportunities in exosome research—perspectives from biology, engineering, and cancer therapy *APL Bioeng.* **3** 011503

[13] Yang D, Zhang W, Zhang H, Zhang F, Chen L, Ma L, Larcher L M, Chen S, Liu N and Zhao Q 2020 Progress, opportunity, and perspective on exosome isolation-efforts for efficient exosome-based theranostics *Theranostics* **10** 3684

[14] Kojima R, Bojar D, Rizzi G, Hamri G C E, El-Baba M D, Saxena P, Auslander S, Tan K R and Fussenegger M 2018 Designer exosomes produced by implanted cells intracerebrally deliver therapeutic cargo for Parkinson's disease treatment *Nat. Commun.* **9** 1305

[15] Headland S E, Jones H R, D'Sa A S V, Perretti M and Norling L V 2014 Cutting-edge analysis of extracellular microparticles using ImageStream(X) imaging flow cytometry *Sci. Rep.* **4** 5237

[16] Pick H, Schmid E L, Tairi A P, Ilegems E, Hovius R and Vogel H 2005 Investigating cellular signaling reactions in single attoliter vesicles *J. Am. Chem. Soc.* **127** 2908–12

[17] Momen-Heravi F, Bala S, Kodys K and Szabo G 2015 Exosomes derived from alcohol-treated hepatocytes horizontally transfer liver specific miRNA-122 and sensitize monocytes to LPS *Sci. Rep.* **5** 09991

[18] Sun L, Wang H X, Zhu X J, Wu P H, Chen W Q, Zou P, Li Q B and Chen Z C 2014 Serum deprivation elevates the levels of microvesicles with different size distributions and selectively enriched proteins in human myeloma cells *in vitro* *Acta Pharmacol. Sin.* **35** 381–93

[19] King H W, Michael M Z and Gleadle J M 2012 Hypoxic enhancement of exosome release by breast cancer cells *BMC Cancer* **12** 421

[20] Piffoux M, Nicolas-Boluda A, Mulens-Arias V, Richard S, Rahmi G, Gazeau F, Wilhelm C and Silva A K A 2019 Extracellular vesicles for personalized medicine: the input of physically triggered production, loading and theranostic properties *Adv. Drug Deliv. Rev.* **138** 247–58

[21] Fruhbeis C, Helmig S, Tug S, Simon P and Kramer-Albers E M 2015 Physical exercise induces rapid release of small extracellular vesicles into the circulation *J. Extracell. Vesicles* **4** 28239

[22] Ito Y *et al* 2018 Turbulence activates platelet biogenesis to enable clinical scale ex vivo production *Cell* **174** 636

[23] Vion A C, Ramkhelawon B, Loyer X, Chironi G, Devue C, Loirand G, Tedgui A, Lehoux S and Boulanger C M 2013 Shear stress regulates endothelial microparticle release *Circ. Res.* **112** 1323

[24] Wang Z Y, Maruyama K, Sakisaka Y, Suzuki S, Tada H, Suto M, Saito M, Yamada S and Nemoto E 2019 Cyclic stretch force induces periodontal ligament cells to secrete exosomes that suppress IL-1 beta production through the inhibition of the NF-kappa B signaling pathway in macrophages *Front. Immunol.* **10** 1310

[25] Yan L, Liu G and Wu X 2021 Exosomes derived from umbilical cord mesenchymal stem cells in mechanical environment show improved osteochondral activity via upregulation of LncRNA H19 *J. Orthop. Transl.* **26** 111–20

[26] Najrana T, Mahadeo A, Abu-Eid R, Kreienberg E, Schulte V, Uzun A, Schorl C, Goldberg L, Quesenberry P and Sanchez-Esteban J 2020 Mechanical stretch regulates the expression of specific miRNA in extracellular vesicles released from lung epithelial cells *J. Cell. Physiol.* **235** 8210–23

[27] Yu W J, Chen C D, Kou X X, Sui B D, Yu T T, Liu D W, Wang R C, Wang J and Shi S T 2021 Mechanical force-driven TNF alpha endocytosis governs stem cell homeostasis *Bone Res.* **8** 44

[28] Deng Z T, Wang J Q, Xiao Y, Li F, Niu L, Liu X, Meng L and Zheng H R 2021 Ultrasound-mediated augmented exosome release from astrocytes alleviates amyloid-beta-induced neurotoxicity *Theranostics* **11** 4351–62

[29] Ambattu L A, Ramesan S, Dekiwadia C, Hanssen E, Li H Y and Yeo L S Y 2020 High frequency acoustic cell stimulation promotes exosome generation regulated by a calcium-dependent mechanism *Commun. Biol.* **3** 553

[30] Guo S W *et al* 2021 Stimulating extracellular vesicles production from engineered tissues by mechanical forces *Nano Lett.* **21** 2497–504

[31] Balachandar S and Eaton J K 2010 Turbulent dispersed multiphase flow *Annu. Rev. Fluid Mech.* **42** 111–33

[32] Livak K J and Schmittgen T D 2001 Analysis of relative gene expression data using real-time quantitative PCR and the 2(T)(-Delta Delta C) method *Methods* **25** 402–8

[33] Baietti M F *et al* 2012 Syndecan-syntenin-ALIX regulates the biogenesis of exosomes *Nat. Cell Biol.* **14** 677–85

[34] Zhao X, Lang Q, Yildirimer L, Lin Z Y, Cui W G, Annabi N, Ng K W, Dokmeci M R, Ghaemmaghami A M and Khademhosseini A 2016 Photocrosslinkable gelatin hydrogel for epidermal tissue engineering *Adv. Healthcare Mater.* **5** 108–18

[35] Zhao X, Liu S, Yildirimer L, Zhao H, Ding R H, Wang H N, Cui W G and Weitz D 2016 Injectable stem cell-laden photocrosslinkable microspheres fabricated using microfluidics for rapid generation of osteogenic tissue constructs *Adv. Funct. Mater.* **26** 2809–19

[36] Hengartner M O 2000 The biochemistry of apoptosis *Nature* **407** 770–6

[37] Elfenbein A and Simons M 2013 Syndecan-4 signaling at a glance *J. Cell. Sci.* **126** 3799–804

[38] Thery C *et al* 2018 Minimal information for studies of extracellular vesicles 2018 (MISEV2018): a position statement of the international society for extracellular vesicles and update of the MISEV2014 guidelines *J. Extracell. Vesicles* **7** 1535750

[39] Im E J *et al* 2019 Sulfisoxazole inhibits the secretion of small extracellular vesicles by targeting the endothelin receptor A *Nat. Commun.* **10** 1387

[40] Trapani J A 1995 Target cell apoptosis induced by cytotoxic T cells and natural killer cells involves synergy between the pore-forming protein, perforin, and the serine protease, granzyme B *Aust. N. Z. J. Med.* **25** 793–9

[41] Lugini L *et al* 2012 Immune surveillance properties of human NK cell-derived exosomes *J. Immunol.* **189** 2833–42

[42] Bei H P, Hung P M, Yeung H L, Wang S and Zhao X 2021 Bone-a-Petite: engineering exosomes towards bone, osteochondral, and cartilage repair *Small* **17** 50

[43] Lee J H, Choi J H, Chueng S T D, Pongkulapa T, Yang L T, Cho H Y, Choi J W and Lee K B 2019 Nondestructive characterization of stem cell neurogenesis by a

magneto-plasmonic nanomaterial-based exosomal miRNA detection *ACS Nano* **13** 8793–803
[44] Grapp M *et al* 2013 Choroid plexus transcytosis and exosome shuttling deliver folate into brain parenchyma *Nat. Commun.* **4** 2123
[45] Xie F, Zhou X X, Fang M Y, Li H Y, Tu Y F, Su P, Zhang L and Zhou F F 2019 Extracellular vesicles in cancer immune microenvironment and cancer immunotherapy *Adv. Sci.* **6** 1901779
[46] Liang L G *et al* 2017 An integrated double-filtration microfluidic device for isolation, enrichment and quantification of urinary extracellular vesicles for detection of bladder cancer *Sci. Rep.* **7** 46224
[47] Vining K H and Mooney D J 2017 Mechanical forces direct stem cell behaviour in development and regeneration *Nat. Rev. Mol. Cell Biol.* **18** 728–42
[48] Diehl P, Nagy F, Sossong V, Helbing T, Beyersdorf F, Olschewski M, Bode C and Moser M 2008 Increased levels of circulating microparticles in patients with severe aortic valve stenosis *Thromb. Haemost.* **99** 711–9
[49] Miyazaki Y, Nomura S, Miyake T, Kagawa H, Kitada C, Taniguchi H, Komiyama Y, Fujimura Y, Ikeda Y and Fukuhara S 1996 High shear stress can initiate both platelet aggregation and shedding of procoagulant containing microparticles *Blood* **88** 3456–64
[50] Schmoranzer J, Kreitzer G and Simon S M 2003 Migrating fibroblasts perform polarized, microtubule-dependent exocytosis towards the leading edge *J. Cell. Sci.* **116** 4513–9
[51] Gauthier N C, Fardin M A, Roca-Cusachs P and Sheetz M P 2011 Temporary increase in plasma membrane tension coordinates the activation of exocytosis and contraction during cell spreading *Proc. Natl Acad. Sci. USA* **108** 14467–72
[52] Groulx N, Boudreault F, Orlov S N and Grygorczyk R 2006 Membrane reserves and hypotonic cell swelling *J. Membr. Biol.* **214** 43–56
[53] Morrell A E *et al* 2018 Mechanically induced Ca_2+ oscillations in osteocytes release extracellular vesicles and enhance bone formation *Bone Res.* **6** 6
[54] Nguyen R *et al* 2019 A phase II clinical trial of adoptive transfer of haploidentical natural killer cells for consolidation therapy of pediatric acute myeloid leukemia *J. Immunother. Cancer* **7** 81
[55] Vela M *et al* 2018 Haploidentical IL-15/41BBL activated and expanded natural killer cell infusion therapy after salvage chemotherapy in children with relapsed and refractory leukemia *Cancer Lett.* **422** 107–17
[56] Rubnitz J E, Inaba H, Ribeiro R C, Pounds S, Rooney B, Bell T, Pui C H and Wing L 2010 NKAML: a pilot study to determine the safety and feasibility of haploidentical natural killer cell transplantation in childhood acute Myeloid Leukemia *J. Clin. Oncol.* **28** 955–9
[57] Geller M A *et al* 2011 A phase II study of allogeneic natural killer cell therapy to treat patients with recurrent ovarian and breast cancer *Cytotherapy* **13** 98–107
[58] Caldwell K J, Gottschalk S and Talleur A C 2021 Allogeneic CAR cell therapy-more than a pipe dream *Front. Immunol.* **11** 618427
[59] Jong A Y, Wu C H, Li J B, Sun J P, Fabbri M, Wayne A S and Seeger R C 2017 Large-scale isolation and cytotoxicity of extracellular vesicles derived from activated human natural killer cells *J. Extracell. Vesicles* **6** 1294368
[60] Alvarez-Erviti L, Seow Y Q, Yin H F, Betts C, Lakhal S and Wood M J A 2011 Delivery of siRNA to the mouse brain by systemic injection of targeted exosomes *Nat. Biotechnol.* **29** 341–U179